



US Army Corps  
of Engineers  
Waterways Experiment  
Station

AD-A262 366



Technical Report SL-93-1  
January 1993

2

# Analysis of Hopkinson Bar Pressure Gage

by James T. Baylot  
Structures Laboratory

20000920310

Approved For Public Release, Distribution Is Unlimited

Reproduced From  
Best Available Copy

DTIC  
ELECTE  
MAR 13 1993  
S E D

98 3 16 095

93-05474



Prepared for Defense Nuclear Agency

The contents of this report are not to be used for advertising, publication, or promotional purposes. Citation of trade names does not constitute an official endorsement or approval of the use of such commercial products.



PRINTED ON RECYCLED PAPER

Technical Report SL-93-1  
January 1993

# Analysis of Hopkinson Bar Pressure Gage

by James T. Baylot  
Structures Laboratory

U.S. Army Corps of Engineers  
Waterways Experiment Station  
3909 Halls Ferry Road  
Vicksburg, MS 39180-6199

|                    |                                     |
|--------------------|-------------------------------------|
| Accession For      |                                     |
| NTIS CRA&I         | <input checked="" type="checkbox"/> |
| DTIC TAB           | <input checked="" type="checkbox"/> |
| Unannounced        | <input type="checkbox"/>            |
| Justification      |                                     |
| By                 |                                     |
| Distribution/      |                                     |
| Availability Codes |                                     |
| Dist               | Avail and/or Special                |
| A-1                |                                     |

Final report

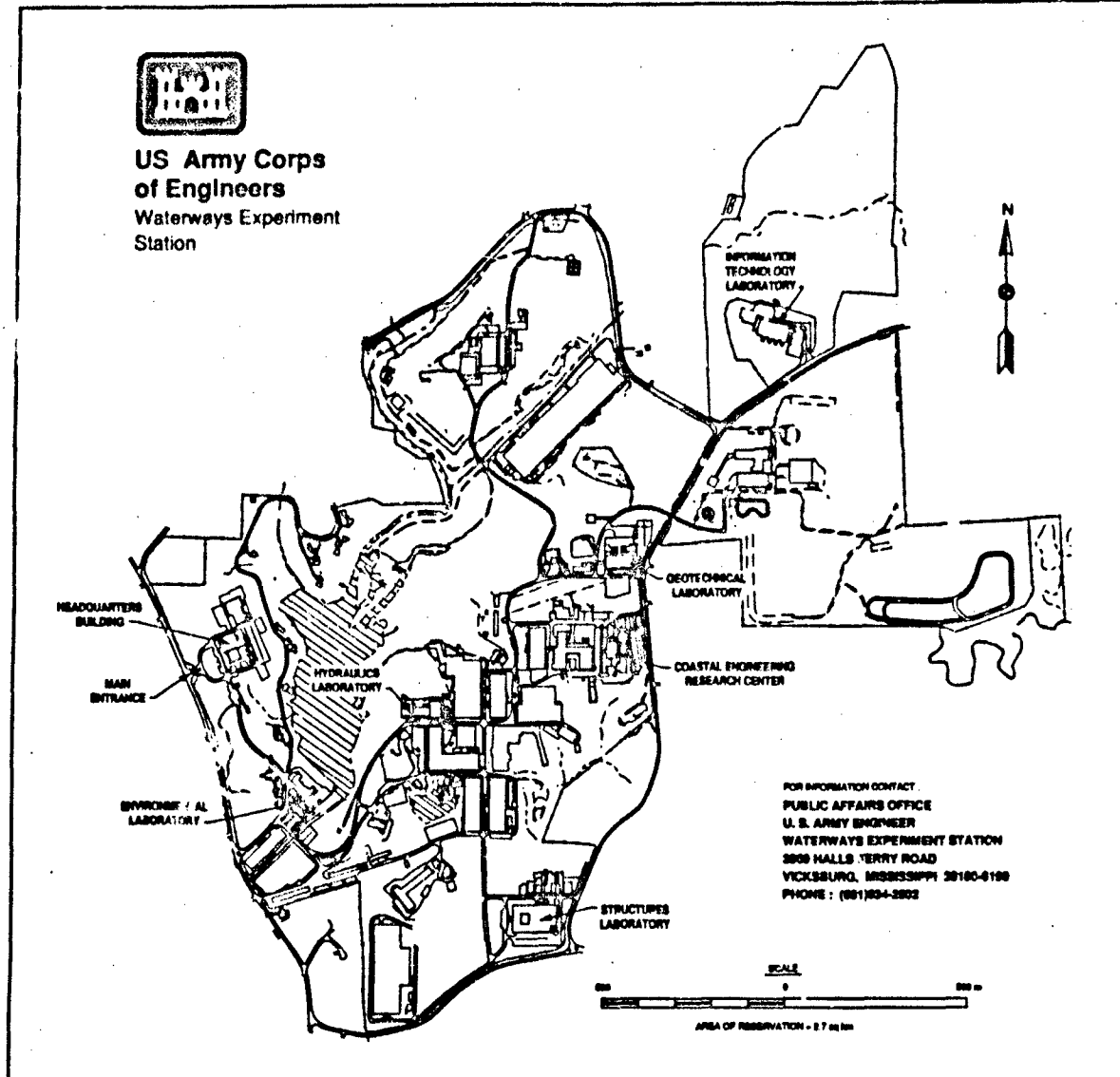
Approved for public release; distribution is unlimited

Prepared for Defense Nuclear Agency  
Washington, DC 20305-1000

Under Subtask RS RC/Missile System Vulnerability  
Work Unit 10186  
and Project H42KRHRD, Work Unit 80850



**US Army Corps  
of Engineers  
Waterways Experiment  
Station**



FOR INFORMATION CONTACT:  
PUBLIC AFFAIRS OFFICE  
U. S. ARMY ENGINEER  
WATERWAYS EXPERIMENT STATION  
8808 HALLS TERRY ROAD  
VICKSBURG, MISSISSIPPI 39180-6198  
PHONE: (601)934-2802

**Waterways Experiment Station Cataloging-in-Publication Data**

Baylot, James T.

Analysis of Hopkinson bar pressure gage / by James T. Baylot ;  
prepared for Department of the Army, U.S. Army Corps of Engineers.  
66 p. : ill. ; 28 cm. — (Technical report ; SL-93-1)

Includes bibliographical references.

1. Pressure gages. 2. Blast effect — Measurement — Instruments.
3. Detonation waves — Measurement — Instruments. 4. Shock (Mechanics) — Measurements — Instruments. I. United States. Army. Corps of Engineers. II. U.S. Army Engineer Waterways Experiment Station. III. Title. IV. Series: Technical report (U.S. Army Engineer Waterways Experiment Station) ; SL-93-1.

TA7 W34 no.SL-93-1

## PREFACE

This report documents the analyses performed to assess the accuracy of Hopkinson bar pressure gages for measuring very high airblast pressures. The research was sponsored jointly by the Defense Nuclear Agency (DNA) under Subtask RS RC/Missile System Vulnerability, Work Unit 10186, "Structures Research Program," and Field Command DNA (FCDNA) under Project H42KRHRD, Work Unit 80850, "Gage Diagnostic Support." Technical Monitors were CPT Mark H. Abernathy, DNA, and CPT Michael B. Scott, FCDNA. Dr. Eric Rinehart, FCDNA, provided much of the initial impetus for this research, as well as valuable suggestions throughout the program.

These analyses were performed in the Structures Laboratory (SL), U.S. Army Engineer Waterways Experiment Station (WES), by Mr. James T. Baylot, Research Structural Engineer, Structural Mechanics Division (SMD), under the general supervision of Messrs. Bryant Mather and James T. Ballard, Director and Assistant Director, SL, respectively; and under the direct supervision of Drs. Jimmy P. Balsara, Chief, SMD, and Robert Hall, Chief, Analysis Group, SMD. Mr. C. Robert Welch, Explosion Effects Division, SL, was the WES manager for the FCDNA portion of this project. This report was prepared by Mr. Baylot.

At the time of publication of this report, Director of WES was Dr. Robert W. Whalin. Commander was COL Leonard G. Hassell, EN.

CONTENTS

|  | <u>Page</u> |
|--|-------------|
| PREFACE . . . . .  | 1           |
| CONVERSION FACTORS, NON-SI TO SI (METRIC) UNITS OF MEASUREMENT . . . . .       | 4           |
| CHAPTER 1 INTRODUCTION. . . . .  | 5           |
| 1.1 BACKGROUND . . . . .   | 5           |
| 1.2 OBJECTIVES . . . . .   | 7           |
| 1.3 SCOPE. . . . .   | 8           |
| CHAPTER 2 RESPONSE OF WES BAR, BAR ONLY . . . . .                              | 12          |
| 2.1 PRELIMINARY CALCULATIONS . . . . .   | 12          |
| 2.2 "EXACT" SOLUTION . . . . .   | 13          |
| 2.3 COMPARISON OF "EXACT" TO FE SOLUTION . . . . .                             | 15          |
| 2.4 RESPONSE OF BAR TO LOADING FROM DET TEST . . . . .                         | 16          |
| 2.5 RESPONSE OF WES BAR TO MINERAL FIND III LOADING. . . . .                   | 18          |
| CHAPTER 3 EFFECT OF WATER AND WATER SEAL. . . . .                              | 28          |
| 3.1 BAR, WATER, AND WATER SEAL . . . . .                                       | 28          |
| 3.2 EFFECT OF WATER VISCOSITY. . . . .   | 30          |
| 3.3 BAR, WATER, WATER SEAL, PVC PIPE, AND SOIL . . . . .                       | 32          |
| CHAPTER 4 COMPARISON OF WES AND NMEPI BARS IN DET<br>DEVELOPMENT TEST. . . . . | 45          |
| 4.1 REASON FOR ANALYSES. . . . .   | 45          |
| 4.2 RESPONSE TO PCB3 LOADING . . . . .   | 47          |
| 4.3 RESPONSE TO PCB2 LOADING . . . . .   | 48          |
| 4.4 OVERALL COMPARISON OF WES AND NMEPI BAR GAGES. . . . .                     | 49          |
| CHAPTER 5 SUMMARY, CONCLUSIONS, AND RECOMMENDATIONS . . . . .                  | 54          |
| 5.1 SUMMARY . . . . .  | 54          |
| 5.2 CONCLUSIONS . . . . .  | 55          |
| 5.3 RECOMMENDATIONS . . . . .  | 57          |
| REFERENCES . . . . .   | 58          |

LIST OF FIGURES

| <u>Figure</u> |   | <u>Page</u> |
|---------------|---|-------------|
| 1.1           | Cross section of WES bar gage. . . . .  | 10          |
| 1.2           | Comparison of WES to PCB gage data,<br>DET development test . . . . .                         | 10          |
| 1.3           | Comparison of averaged bar gage to averaged<br>Kulite gage for Mineral Find III test. . . . . | 11          |
| 1.4           | Comparison of WES to NMERI bar data,<br>DET development test . . . . .                        | 11          |
| 2.1           | Loading for preliminary calculations . . . . .  | 20          |
| 2.2           | Cross sections of grids. . . . .  | 20          |
| 2.3           | Results of preliminary calculations. . . . .  | 21          |
| 2.4           | Comparison of simple solution to FE solution . . . . .  | 21          |
| 2.5           | Wave speed ratio based on "exact" solution . . . . .  | 22          |
| 2.6           | Fit to airblast pressure data. . . . .  | 22          |
| 2.7           | Comparison of PCB2 data to Fourier series fit. . . . .  | 23          |
| 2.8           | Comparison of "exact" to FE solution, PCB2 loading . . . . .                                  | 23          |
| 2.9           | Comparison of "exact" to FE solution, PCB5 loading . . . . .                                  | 24          |
| 2.10          | Comparison of "exact" to FE solution<br>averaged Kulite loading. . . . .                      | 24          |
| 2.11          | Comparison of "exact" to FE solution,<br>NMERI bar, PCB3 loading. . . . .                     | 25          |
| 2.12          | Comparison of PCB2, W2, and "exact" solution . . . . .  | 25          |
| 2.13          | Comparison of W2 to filtered solutions . . . . .  | 26          |
| 2.14          | Frequency content of PCB2, PCB5, W2. . . . .  | 26          |
| 2.15          | Comparison of filtered and unfiltered solutions,<br>averaged Kulite. . . . .                  | 27          |
| 2.16          | Frequency content of averaged Kulite<br>and bar gage data. . . . .                            | 27          |
| 3.1           | Water added to grid. . . . .  | 40          |
| 3.2           | Early-time comparison of stresses<br>with and without water . . . . .                         | 40          |
| 3.3           | Comparison of bar stresses with and without water. . . . .                                    | 41          |
| 3.4           | Velocity profile for viscosity calculations. . . . .  | 41          |
| 3.5           | Velocities of top and bottom of water. . . . .  | 42          |
| 3.6           | Relative displacement at top of bar. . . . .  | 42          |
| 3.7           | Section of grid including PVC pipe and soil. . . . .  | 43          |
| 3.8           | Bar stresses computed using entire grid. . . . .  | 43          |
| 3.9           | Spacer block . . . . .  | 44          |
| 4.1           | Comparison of PCB3 to N4 and "exact"<br>solution for NMERI bar . . . . .                      | 50          |
| 4.2           | Comparison of N4 with "exact" and<br>filtered "exact" solutions . . . . .                     | 50          |
| 4.3           | Fourier series coefficients for PCB3 and N4. . . . .  | 51          |
| 4.4           | Comparison of PCB3 to "exact" solutions<br>for WES and NMERI bars . . . . .                   | 51          |
| 4.5           | Filtered "exact" solution for WES bar, PCB3 loading. . . . .                                  | 52          |
| 4.6           | PCB2, "exact" solutions for WES and NMERI bars . . . . .                                      | 52          |
| 4.7           | PCB2 filtered "exact" solutions for WES and NMERI bars . . . . .                              | 53          |

CONVERSION FACTORS, NON-SI TO SI (METRIC)  
UNITS OF MEASUREMENT

Non-SI units of measurement used in this report can be converted to SI (metric) units as follows:

| <u>Multiply</u>                | <u>By</u>   | <u>To Obtain</u>             |
|--------------------------------|-------------|------------------------------|
| feet                           | 0.3048      | metres                       |
| inches                         | 25.4        | millimetres                  |
| pounds (force)                 | 4.47222     | newtons                      |
| pounds (force) per square inch | 0.006894757 | megapascals                  |
| pounds (mass)                  | 0.4535924   | kilograms                    |
| pounds (mass) per cubic foot   | 16.01846    | kilograms per<br>cubic metre |

## Analysis of Hopkinson Bar Pressure Gage

### CHAPTER 1

#### INTRODUCTION

##### 1.1 BACKGROUND

In order to fully understand the results of experiments on buried structures subjected to high intensity airblast that simulates nuclear weapons effects, an accurate measurement of the airblast pressure time-history must be made. Quite often, the peak airblast pressures in these tests are above what commercially-available air-pressure gages are capable of measuring. Hopkinson bar pressure gages remain elastic while measuring these very high airblast pressures. These bar gages also have the advantage that the sensing element of the gage is placed at a distance down the bar from the high pressure airblast. Thus the sensing element and the wires attached to it stand a much better chance of surviving the environment created by the simulator.

The U.S. Army Engineer Waterways Experiment Station (WES) has developed a bar gage, Figure 1.1, designed to measure the airblast for tests in which airblast-induced ground shock is simulated. The WES bar gage is an approximately 20-ft-long<sup>1</sup>, 1-in.-diameter, high-strength steel bar. The bar is placed inside of a 2-in.-diameter polyvinyl chloride (PVC) pipe to isolate the bar from the surrounding soil. A seal is placed around the bar and

---

<sup>1</sup>A table of factors for converting non-SI to SI (metric) units of measurement is presented on page 4.

inside the PVC pipe at a distance of 4 ft from the top of the bar. The top 4 ft of the space between the bar and the PVC is then filled with water. This prevents the airblast pressure from entering the gap between the bar and pipe and destroying the sensing element before the measurement can be made. Strain gages are placed on machined flats 6 ft down from the top of the bar. These gages measure the vertical and circumferential strains in the bar and are used to compute the vertical stress.

This bar gage design has been used in numerous tests and is still being used. In most of these tests, these bar gages have provided the only estimates of the magnitude of the peak pressure. In the Dilute Explosive Tile (DET) Development Test [1], recently modified Model 109A quartz high-pressure transducers manufactured by PCB Piezotronics, Inc., have been shown to be effective and survivable in these very high airblast pressure environments. In this test, several PCB gages and several WES bar gages were fielded. In the Mineral Find III test [2], both WES bar gages and Model HKS11375 airblast pressure gages manufactured by Kulite were used to measure the airblast.

Although data were limited in these tests, several trends were distinguishable. As shown in Figure 1.2 the peak pressure, as measured by one of the WES bar gages in the DET test, is significantly lower than that measured by one of the PCB gages. Figure 1.3 shows that the peak pressure, as measured by the bar gage in Mineral Find III, is lower than the peak pressure measured by the Kulite gage. In this figure averaged bar gage results are compared to averaged Kulite results. In computing these averages, records which were obviously bad or which were inconsistent with the other records were not included.

In the Mineral Find I and Mineral Find II tests [20], this trend did not hold. In these tests the peak pressures measured by the bar gages were higher than those measured by the Kulite gages. Although these tests will not be analyzed in this study the reversal of this trend is certainly significant.

Later in time, the peak pressure measured by the bar gage is higher than that measured by the PCB gage in the DET test. The same trend occurs when comparing the averaged bar gage record to the averaged Kulite pressure gage record in the Mineral Find III test.

Several bar gages were fielded by the New Mexico Engineering Research Institute (NMERI) on the DET tests. The primary difference between the WES and NMERI bars is that the WES and NMERI bars have 1.0 and 0.5 in, diameters, respectively. A comparison of one of the NMERI bar gage records to one of the WES bar records is given in Figure 1.4. Five WES and five NMERI bars were placed under the DET Section of the test bed. All five of the WES bar gages displayed a single dominant peak, while all NMERI bars reveal two dominant peaks. Two of the five PCB gage records showed a single-peaked pressure time-history, and two showed a double-peaked pressure time-history. One PCB gage failed very early. One WES bar and one NMERI bar were placed in a portion of the test bed which was not under the DET. The characters of the pressure time-histories for these two gages were similar.

## 1.2 OBJECTIVES

The primary objective of this study was to determine the accuracy of the WES bar gage and the possible effects the water and water seal have on the measured waveforms. Other objectives are to evaluate the differences in

measured stresses be on the WES and NMERI bars in the DET test, and to determine if modifications to the WES bar gage design are needed.

### 1.3 SCOPE

Three series of Finite Element (FE) calculations were performed to investigate the response of the bar gage. In the first series, only the steel bar was analyzed. The second series included the bar, the water, and the water seal. The final set of calculations included the bar, water, water seal, PVC pipe, and surrounding soil. FE calculations were performed using the computer code DYNA3D [3]. A theoretical solution was also used to predict the response of the bar alone, and to compare to the first series of FE calculations to determine the accuracy of the FE solutions.

In each analysis of the DET test, the loading applied to the top of the bar was the measured airblast from one of the PCB gages. Two of the PCB gage records, PCB2 and PCB5, were used as the airblast loading in these calculations. In the test bed, the PCB gages were placed very close to two WES bar gages. These bar gages gave very similar output, therefore only one of these gages, gage W2, will be used in the comparisons. In the comparison of the NMERI bar gage to the WES bar gage, bar gage data from gage N4 were used, and data from gage PCB3 were used as the loading. In the analysis of the Mineral Find III data, the averaged Kulite data were used as the loading, and this was compared to the averaged bar gage record.

Each of the gages used in these tests measures the airblast pressure above the gage itself, and not the actual pressure above the ground surface. Differences in the gages and their mounts, and the motions of the mounts could be responsible for differences in measured pressures. Although the PCB

gage and Kulite gage measurements are used as inputs to the bar gage calculations, these measurements cannot be viewed as the correct answer to be compared with bar gage data. These data are a realistic representation of the loading on the top of the bar and can be used to assess the capabilities of the bar gage by comparing the computed bar gage measurements with the load inputs from the PCB and Kulite gage data.

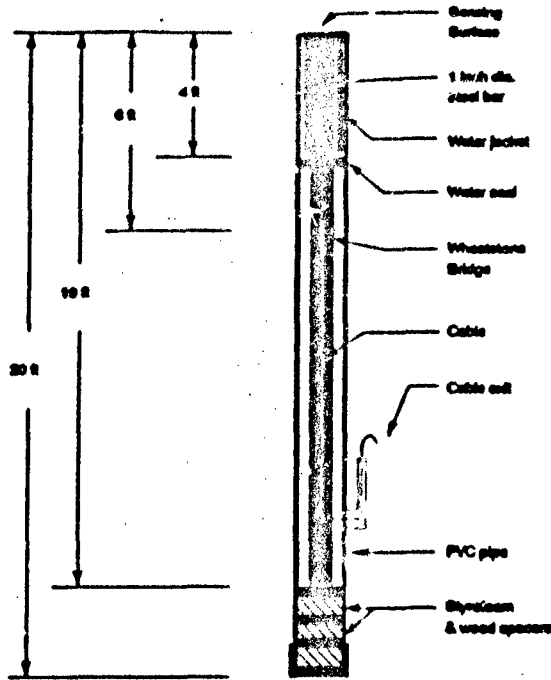


Figure 1.1. Cross section of WES bar gage.

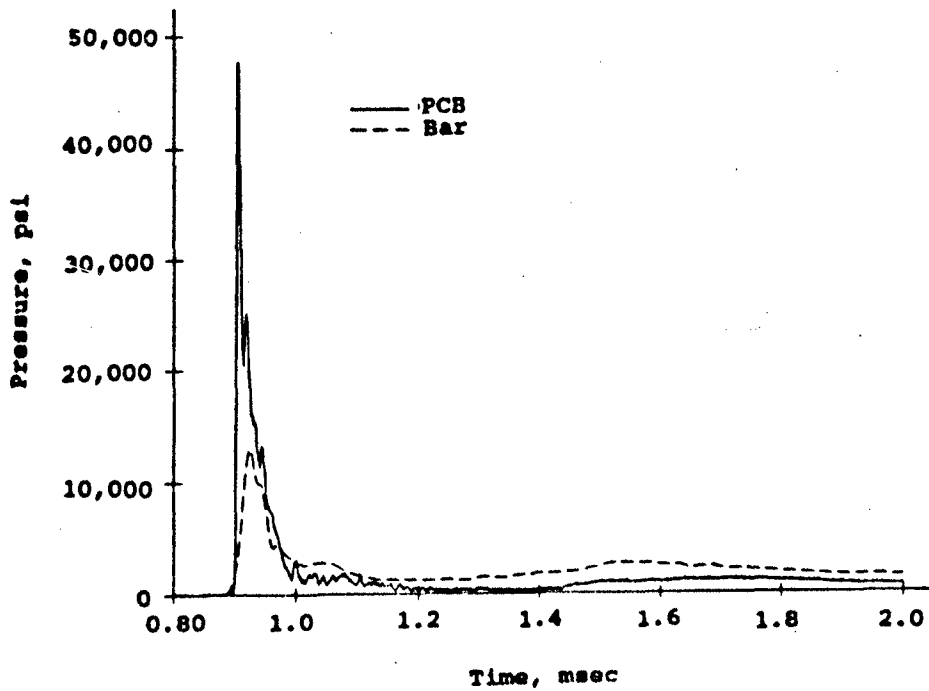


Figure 1.2. Comparison WES bar to PCB gage data, DET development test.

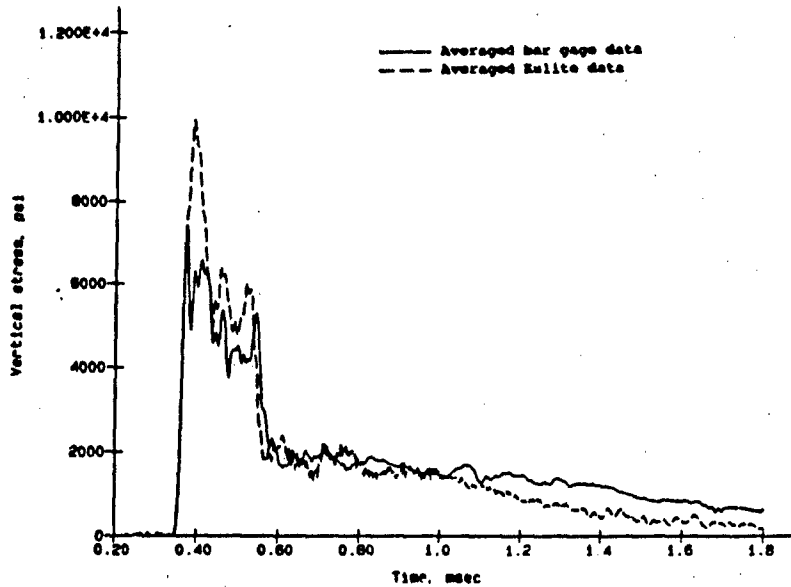


Figure 1.3. Comparison of averaged bar gage to averaged Kulite gage for Mineral Find III test.

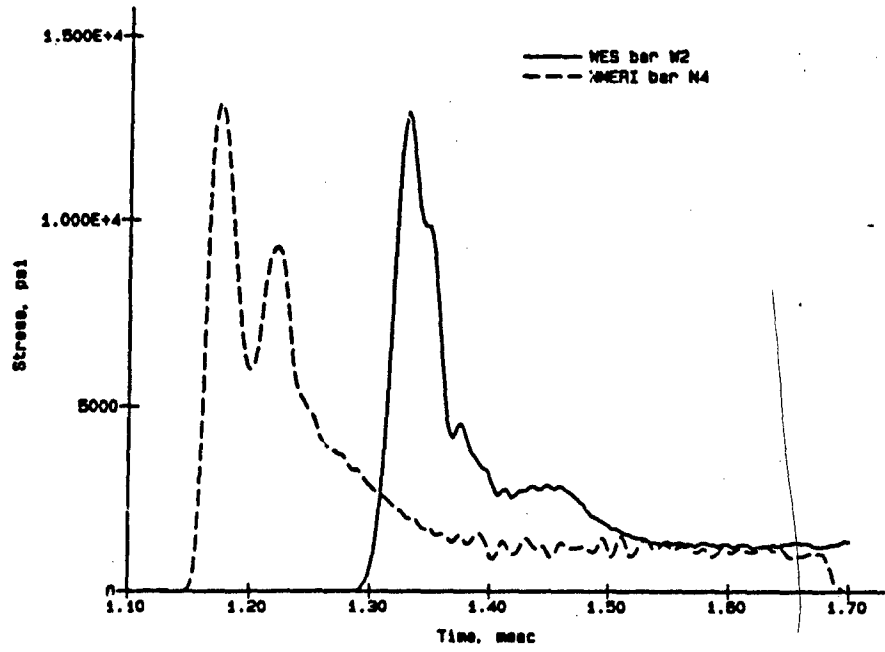


Figure 1.4. Comparison of WES to NMERI bar data, DET development test.

## CHAPTER 2

### RESPONSE OF WES BAR, BAR ONLY

#### 2.1 PRELIMINARY CALCULATIONS

Preliminary calculations were performed to determine the grid size needed to analyze the WES bar gage. In all of the calculations the steel bar was modeled as a linear elastic material with a modulus of elasticity, Poisson's ratio, and unit density of 30,000,000 psi, 0.27, and 490 pcf, respectively. Unless noted otherwise, default values of artificial viscosities and hourglass damping, as well as the standard DYNA3D hourglass control, were used. In those calculations the trilinear pressure time-history shown in Figure 2.1 was used as the loading. Calculations were performed using elements with thicknesses of 1/3, 1/10, and 1/20 in. in the vertical direction. One-fourth of the bar was modeled in each case, and the cross sections of the grids used for each of these calculations are shown in Figure 2.2.

The time-histories for vertical stresses at 4 ft down the bar for each of these calculations are presented in Figure 2.3. The peak stress from the calculation using the 1/10-in.-thick element agrees extremely well with that predicted using the 1/20-in.-thick elements. The peak stress predicted using the 1/3-in.-thick elements is significantly lower than that predicted using the other grids. Later in time there is a difference between the 1/10- and 1/20-in.-thick grids in the period of oscillation of the predicted stress. However, the difference is small and should not affect the results of this study. Therefore, the 1/10 in. elements and the associated grid cross section were selected for use in this study.

## 2.2 "EXACT" SOLUTION

Typically in analyzing bar gage data, it has been assumed that one dimensional (1-D) wave theory is valid. Under these assumptions, the pressure time-history applied to the top of the bar will propagate undistorted down the bar at the longitudinal wave speed,  $c_0 = (E/\rho)^{1/2}$ , of the bar.  $E$  and  $\rho$  are the modulus of elasticity and mass density of the bar, respectively. Figure 2.4 shows that the stress time-history at a distance down the bar can be significantly different than the loading applied at the top of the bar.

When the stress wave propagates down the bar, Poisson strains cause radial motions in the bar. The simple 1-D wave theory assumes that these motions are unimportant. However, for high frequency disturbances, these radial motions can be important. Pochhammer [4] and Chree [5] independently developed a theory, based on the equations of elasticity, which can be used to analyze the bar gage problem. This theory, which includes the effects of radial motion, will be referred to as the "exact" theory. A solution based on Pochhammer-Chree theory for stresses at a great distance from the end of a bar for sinusoidal loads of various frequencies was presented in Love [6], and agreed with results published by Bancroft [7]. This solution indicates that sinusoidal disturbance will propagate undistorted down the bar, but waves of different frequencies will propagate down the bar at different speeds; therefore, dispersion will occur. For high-frequency loadings, the peak stress measured at a distance down a finite-diameter bar will always be less than the applied loading at the top. For longitudinal waves the wave speed,  $c$ , is always less than the 1-D wave propagation speed,  $c_0$ .

This solution is presented in tabular form in Davies [7] for Poisson's ratio = 0.29. In this table the ratio  $c/c_0$  is tabulated against the ratio  $a/W$ .  $W$  and  $a$  are the wavelength of the disturbance and the bar radius, respectively. The wavelength is the wave speed,  $c$ , divided by the frequency,  $f$ , of the disturbance. This table would be more useful if  $c/c_0$  was tabulated against  $a/W_0$ , where  $W_0$  is the wavelength computed using the frequency,  $f$ , and the wave speed,  $c_0$ . Thus the known values of the frequency and 1-D wave speed can be used to determine the value of  $c$ . Figure 2.5 shows the relationship between  $c/c_0$  and  $a/W_0$ .

The following procedure was used to determine the "exact" solution for an arbitrary loading:

1. Determine the full Fourier series coefficients for a pressure time history. The first half of the pressure time-history, Figure 2.6, represents zero magnitude loading for one half a period prior to the application of the loading. The second half of the pressure time history is the arbitrary waveform for which the solution is desired.
2. Calculate the value of  $a/W_{0i}$  for each of the Fourier frequencies,  $f_i$ , and determine the wave speed,  $c_i$ , from Figure 2.5 and the known value of  $c_0$ .
3. Determine the stress time-history at a distance,  $d$ , down the bar by the following superposition:

$$p(t) = 1/2 b_0 + \sum_{i=1}^n [a_i \sin(\omega_i t - L_i) + b_i \cos(\omega_i t - L_i)]$$

Where:  $p(t)$  is the pressure at time,  $t$

$b_0$  is the constant term in the cosine series

$n$  is the number of terms in the series

$w_i$  is  $i^{\text{th}}$  Fourier circular frequency =  $2 \pi f_i$

$a_i$  is the  $i^{\text{th}}$  Fourier sine term

$b_i$  is the  $i^{\text{th}}$  Fourier cosine term

$L_i$  is the lag time for waves of the  $i^{\text{th}}$  frequency

$$L_i = d/c_i$$

A comparison of PCB2 data to the Fourier series using 4,000 terms to fit approximately 1.03 msec of the PCB2 data is shown in Figure 2.7. This figure shows that this is an extremely good representation of the PCB2 data.

Fourier series representations were also determined for gages PCB3 and PCB5 of the DET test and the averaged Kulite record for Mineral Find III. The fits begin at the arrival of the airblast. The durations of the fits are listed below:

| Gage   | Fit Duration<br>(msec) |
|--------|------------------------|
| PCB2   | 1.03                   |
| PCB3   | 0.091                  |
| PCB5   | 2.023                  |
| Kulite | 1.98                   |

### 2.3 COMPARISON OF "EXACT" TO FE SOLUTION

Calculations were performed to determine the exact solution for the stresses at the strain gage location using the PCB2 measurement as the loading. A comparison of the "exact" solution to the FE solution is shown in Figure 2.8. This figure shows that very early in time the FE and "exact" solutions are nearly identical. Later in time there is a difference in the period of the oscillations. This difference could be reduced by using a finer grid mesh, as was shown previously.

Other "exact" and FE analyses were also performed to validate these solutions for different loadings and bar geometries important to this study.

Comparisons of the "exact" theory to FE calculations for the PCB5, and averaged Kulite record loadings are shown in Figures 2.9 and 2.10, respectively. An "exact" solution was also determined for the NMERI bar (0.5-in.-diameter bar, gage 5 ft down bar) using the record from gage PCB3 as the input to the bar. A modified 1/10-in.-thick element grid was used to perform FE calculations of the NMERI bar. The grid was modified by simply scaling the coordinates of the cross section down so that the radius of the bar is 0.25 in. instead of 0.5 in. The vertical dimension of the element remains at 0.1 in. A comparison of the "exact" solution to the FE calculation for the NMERI bar with the PCB3 loading is shown in Figure 2.11.

These calculations showed that for studying the bar alone calculations could be made using either the FE or the "exact" method. The "exact" method is easier and less time consuming, therefore it was used to study the properties of the bar alone. More importantly, this calculation validates the FE procedure so that it can be used for calculations for which exact solutions are not possible. An exact solution that includes the water and water seal is not available.

#### 2.4 RESPONSE OF BAR TO LOADING FROM DET TEST

Figure 2.12 shows a comparison of the input airblast (PCB2 gage measurement) pressure, the exact solution for the bar gage stress, and the W2 data. This figure shows that the peak measured bar stress should be approximately 80 percent of the PCB gage measurement. Thus the peak stress should drop by 20 percent due to dispersion. However, the measured bar gage stress is still significantly less than that.

The W2 data were recorded using electronic cabling and amplifying equipment which provided a frequency response of approximately 20,000 Hz.

The effects of this limited frequency response can be approximated by summing only those Fourier terms with a frequency of less than 20,000 Hz. Figure 2.13 shows a comparison of those predicted stresses at the gage location to the bar gage measurement. This figure shows that the peak stress drops to approximately half of the PCB2 measurement if the frequency response is 20,000 Hz. Thus the lower peak as measured by the bar gages is due largely to the lower frequency response of cabling and electronic systems associated with the bar gages.

Figure 2.14 shows the amplitude,  $(a_i^2 + b_i^2)^{1/2}$ , versus frequency for each term of the Fourier series representation of PCB2, PCB5, and W2. These coefficients are based on the fit durations listed previously for the PCB gages, and a fit duration of 1.03 msec for W2. This figure shows that while the PCB gages indicate significant energy at frequencies above 20,000 Hz, the bar gage does not indicate significant energy above that level. Calculations were also performed for systems with 50,000 and 100,000 Hz frequency response limits. The peak predicted stresses for the 50,000 and 100,000 Hz systems are 10 and 2 percent low, respectively, when compared to the bar response if the recording system had no frequency response limitations.

Also shown in Figure 2.13 is the result of a calculation based on the PCB5 measurement, and using only Fourier series terms with frequencies less than 20,000 Hz. These results agree better with the WES data, and indicate that variability of the environment is a potential source for differences in measured peak stress between the bar gages and the PCB gages.

Figure 2.12 shows that the "exact" solution predicts that oscillations in the measured stress should occur in the bar gage measurement immediately following the arrival of the peak stress. The frequency of these

oscillations is near 50,000 to 60,000 Hz, and it is clear that these oscillations will be severely reduced, if not eliminated, due to the lower frequency response of the recording system. Previous experiments [8] indicate that these oscillations are real, but this can not be evaluated because of the frequency response of the electronics used to record the data. Since both the PCB gage and the bar gage actually measure the airblast pressure on top of a gage and not the airblast applied to the ground surface, it is possible that the gage geometry will affect the measurement. It is also possible that the PCB gages could be overregistering peak pressures. These calculations show that the bar gage and associated recording system cannot adequately record data for an airblast time-history with a fast rise time similar to the pressure time-history recorded on the PCB gages.

#### 2.5 RESPONSE OF WES BAR TO MINERAL FIND III LOADING

Figure 1.3 shows a comparison of the average airblast pressure data recorded for the Kulite gages to the average data recorded for the bar gages. The "exact" solution for the WES bar gage loaded with the averaged Kulite loading indicates that the bar gage should give exactly the same response as the Kulite gage. Therefore Figure 1.3 is also a comparison of the predicted to the measured bar gage stress for this loading. Figure 2.15 shows a comparison of the "exact" solution to the filtered "exact" solution which includes only frequencies below 20,000 Hz. This figure shows that there is no significant difference between the two results. This is expected since the Kulite airblast pressure data were recorded using cabling and recording equipment identical to that used to record the bar data. Thus the frequency response of the Kulite gage is also approximately 20,000 Hz. Figure 2.16 shows a comparison of the magnitudes of the Fourier series components for the

averaged Kulite and averaged bar data. This figure indicates that the frequency response of either gage type for this test was below approximately 20,000 Hz.

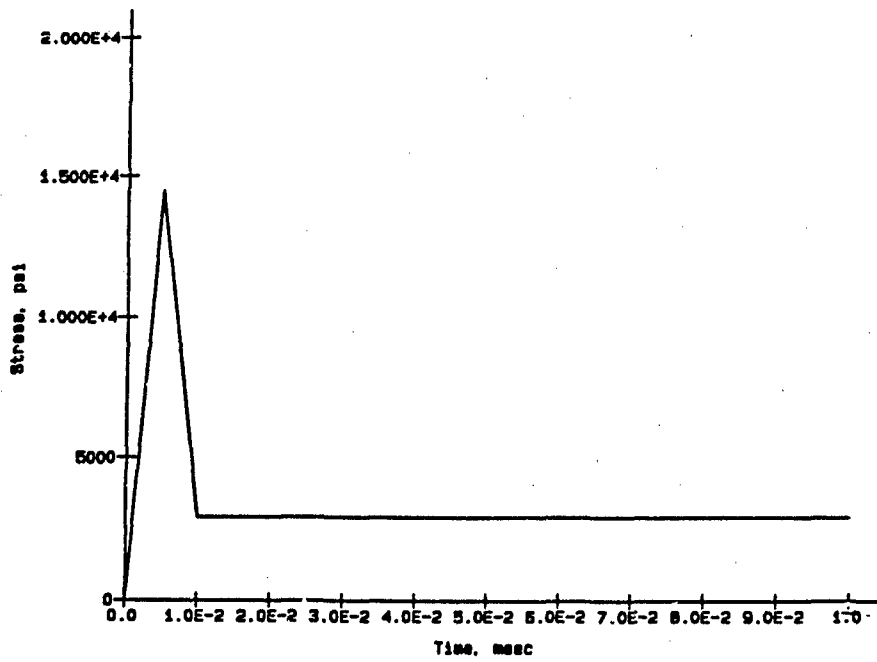
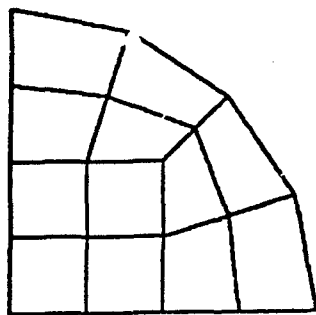
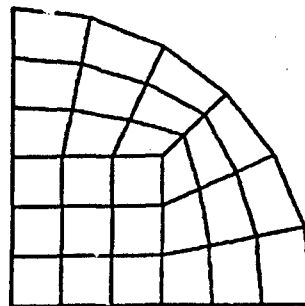


Figure 2.1. Loading for preliminary calculations.



1/10 and 1/3 in. grid



1/20 in. grid

Figure 2.2. Cross sections of grids.

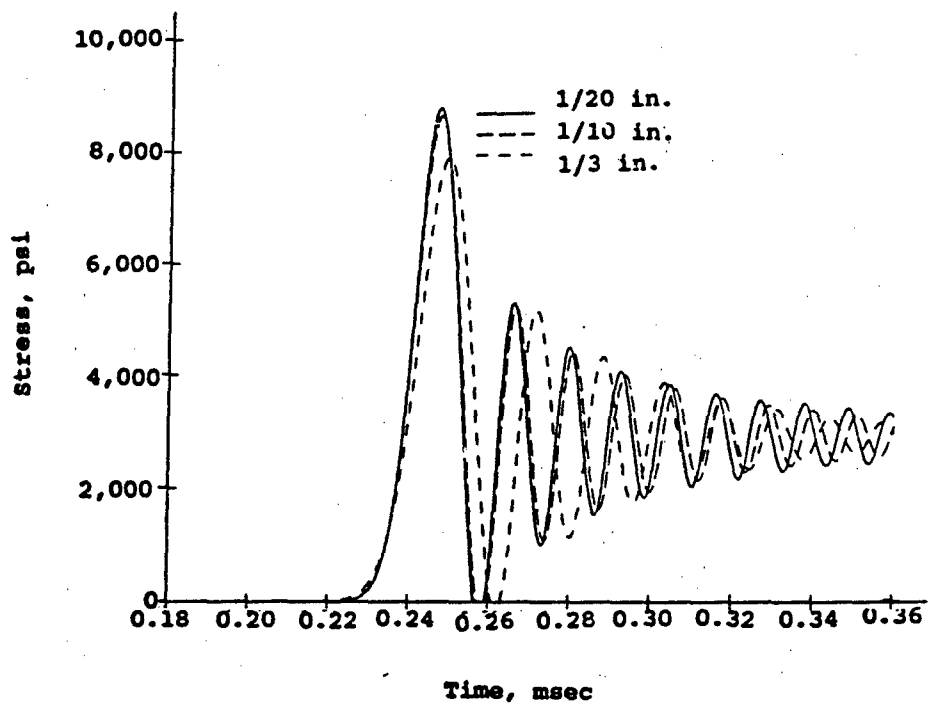


Figure 2.3. Results of preliminary calculations.

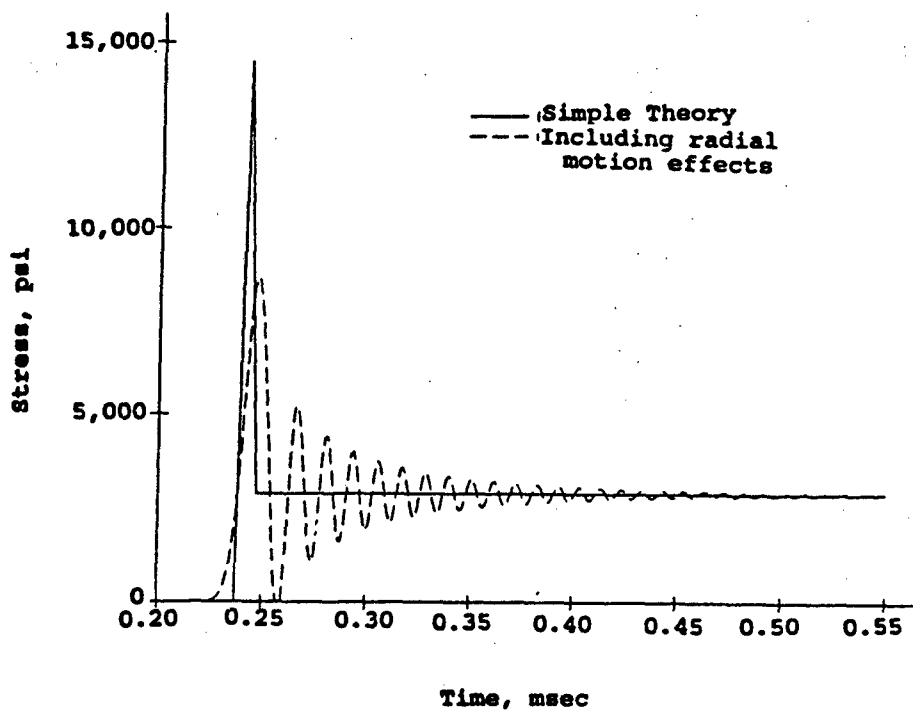


Figure 2.4 Comparison of simple solution to FE solution.

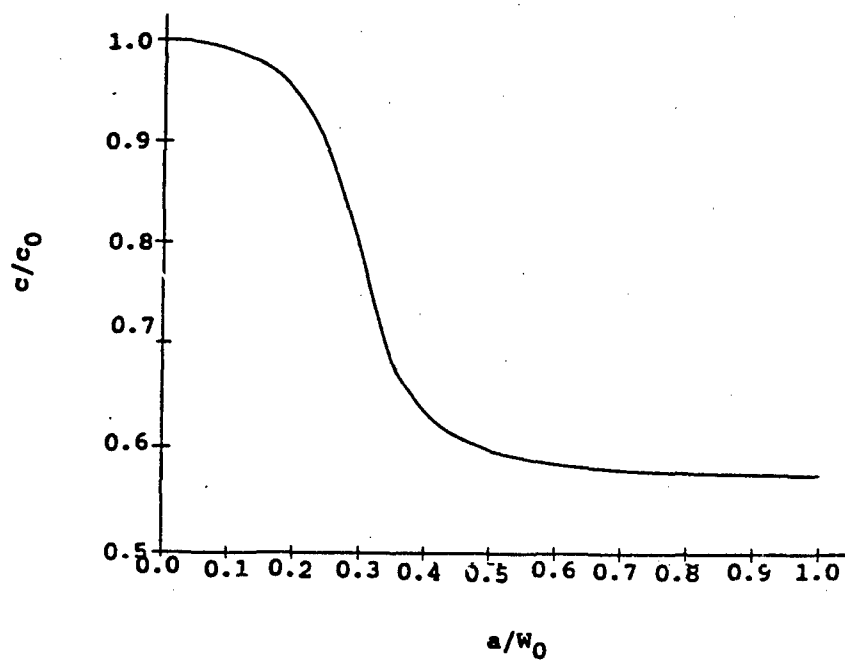


Figure 2.5. Wave speed ratio based on "exact" solution.

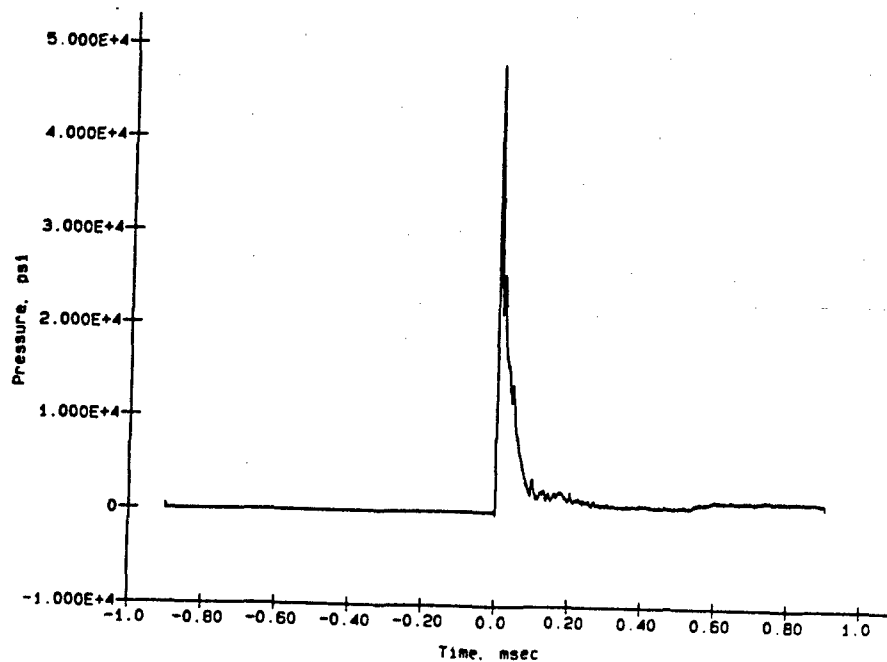


Figure 2.6. Fit to airblast pressure data.

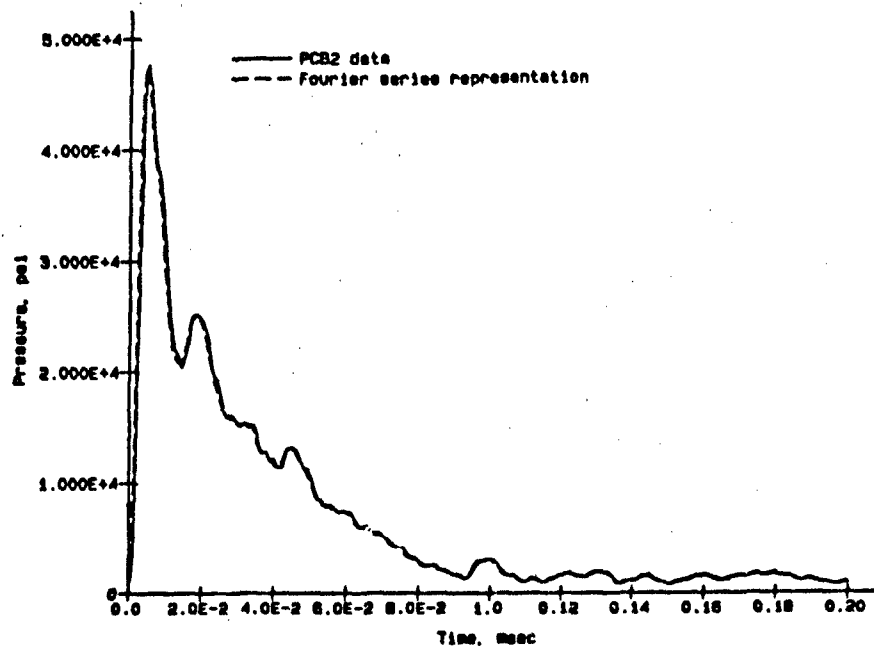


Figure 2.7. Comparison of PCB2 data to Fourier series fit.

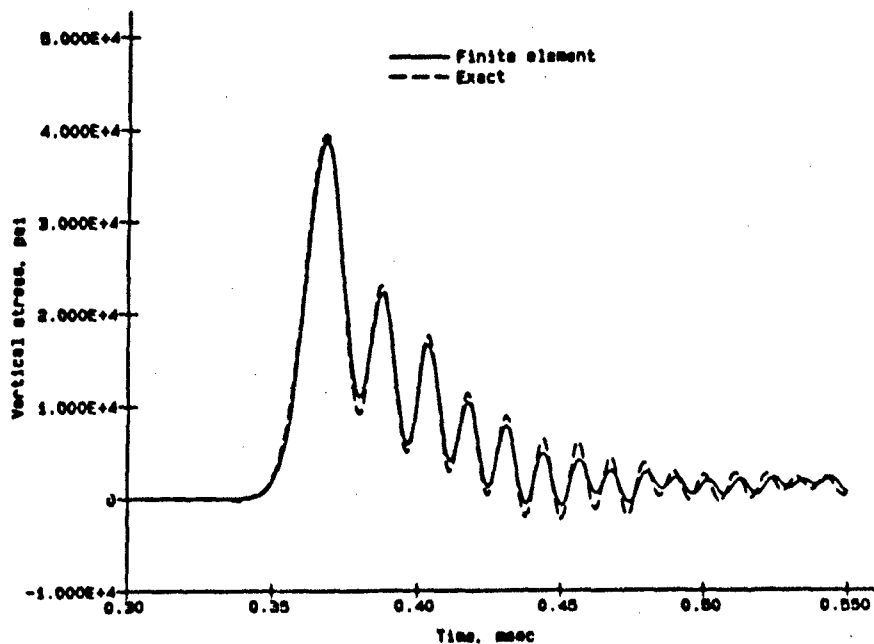


Figure 2.8. Comparison of "exact" to FE solution, PCB2 loading.

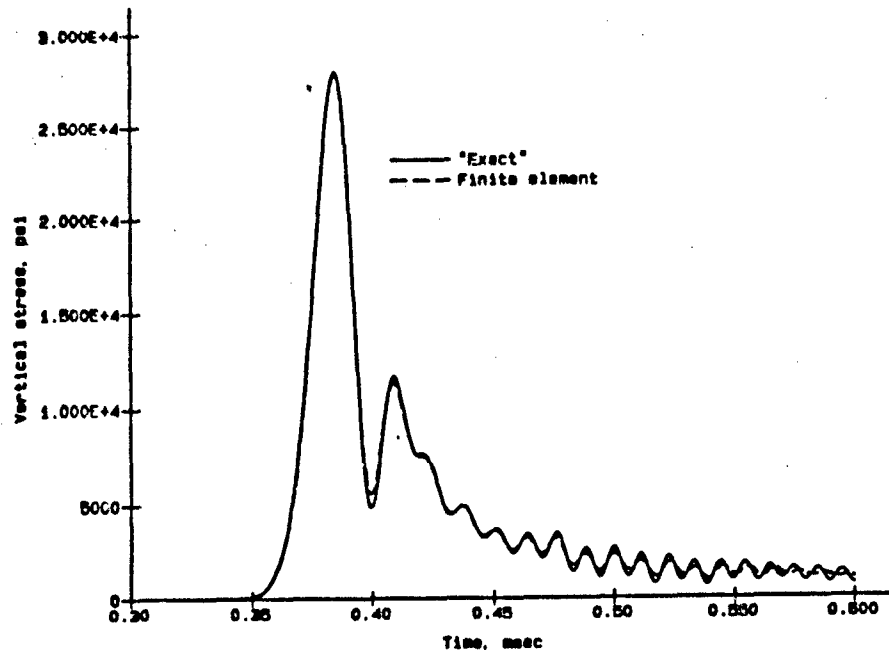


Figure 2.9. Comparison of "exact" to FE solution, PCB5 loading.

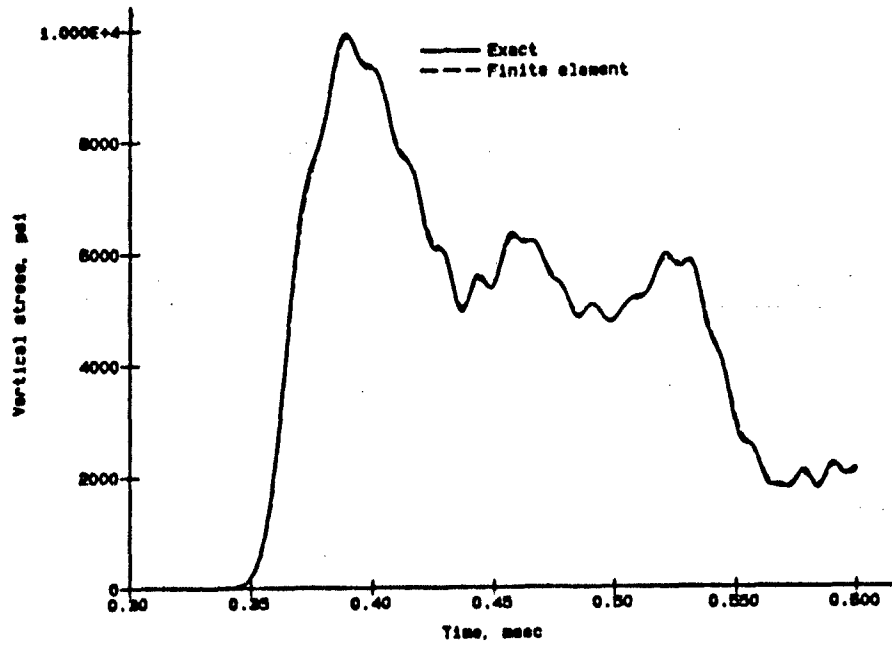


Figure 2.10. Comparison of "exact" to FE solution, averaged Kulite loading.

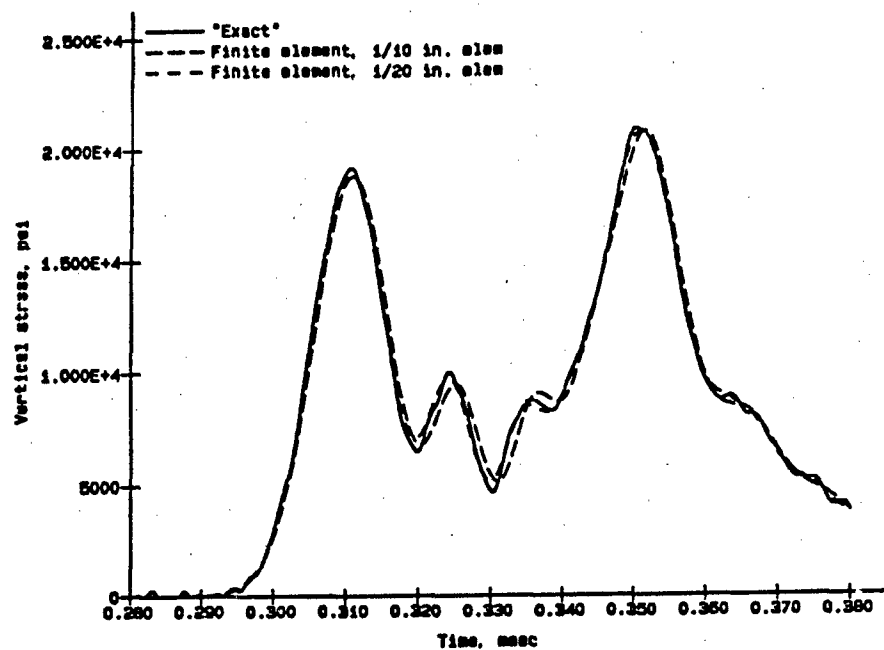


Figure 2.11. Comparison of "exact" to FE solution, NMERI bar, PCB3 loading.

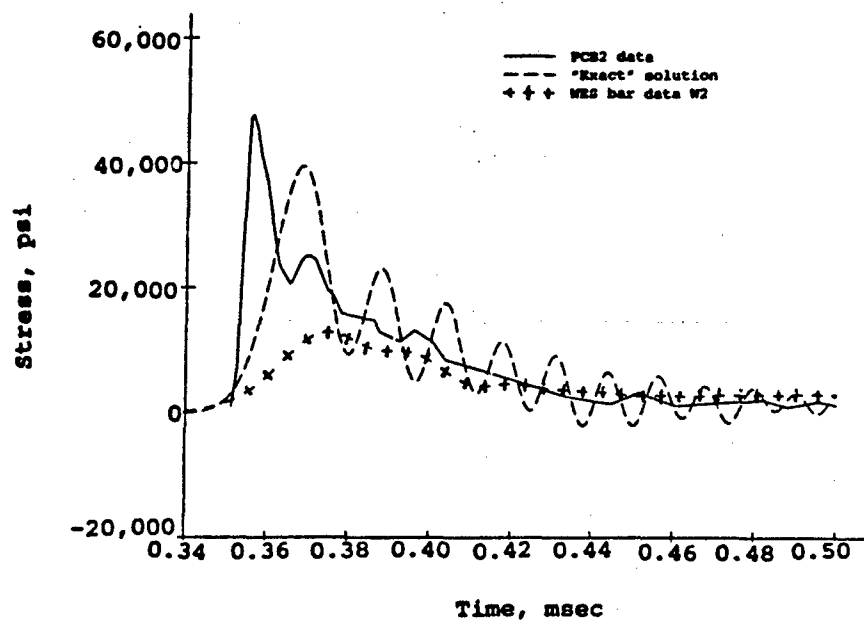


Figure 2.12. Comparison of PCB2, W2, and exact solution.

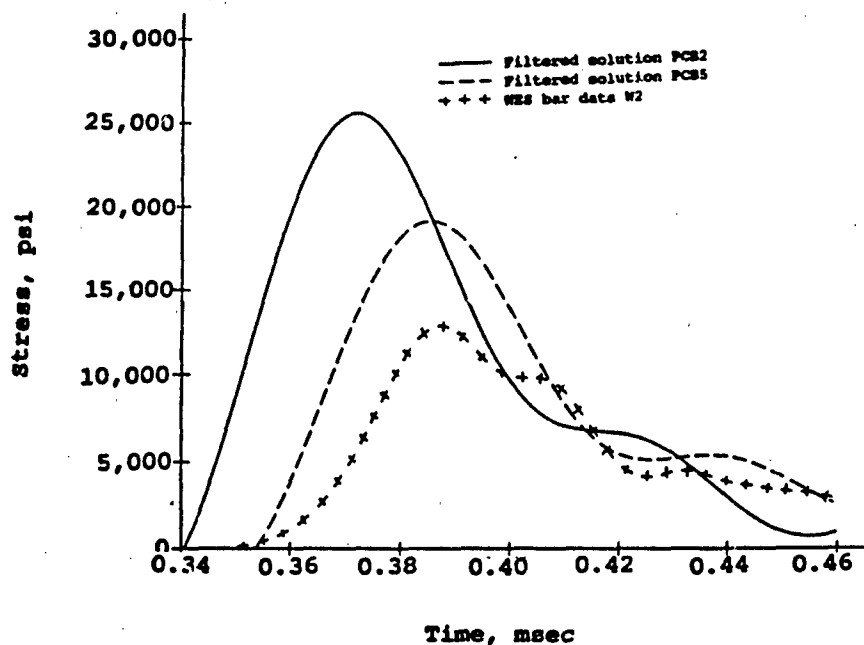


Figure 2.13. Comparison of W2 to filtered solutions.

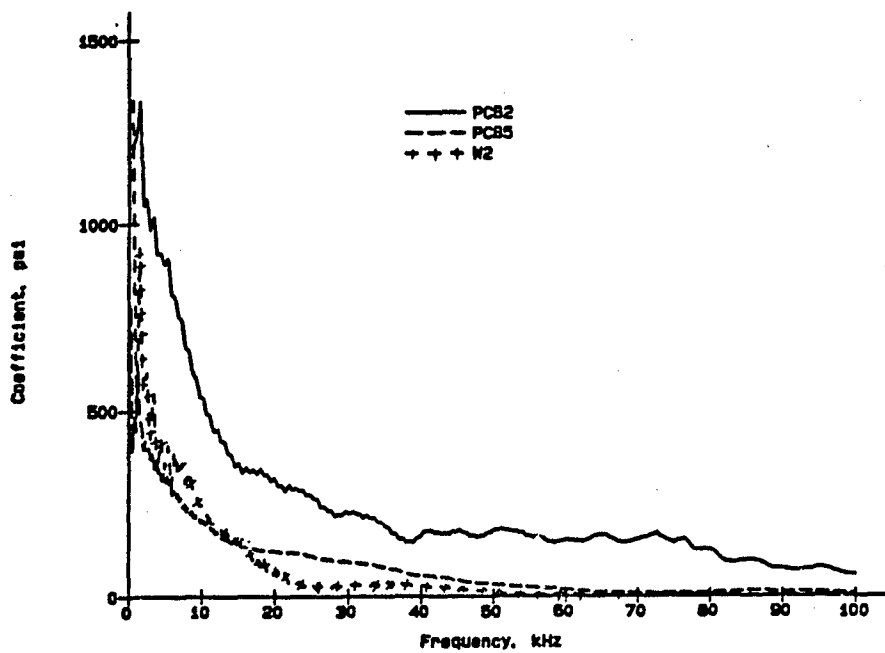


Figure 2.14. Frequency content of PCB2, PCB5, W2.

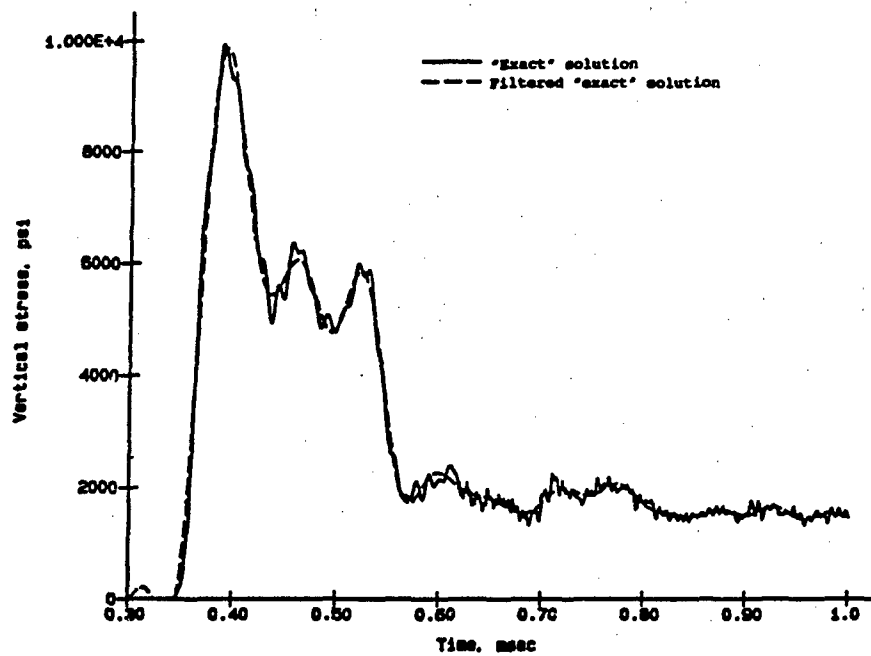


Figure 2.15. Comparison of filtered and unfiltered solutions, averaged Kulite.

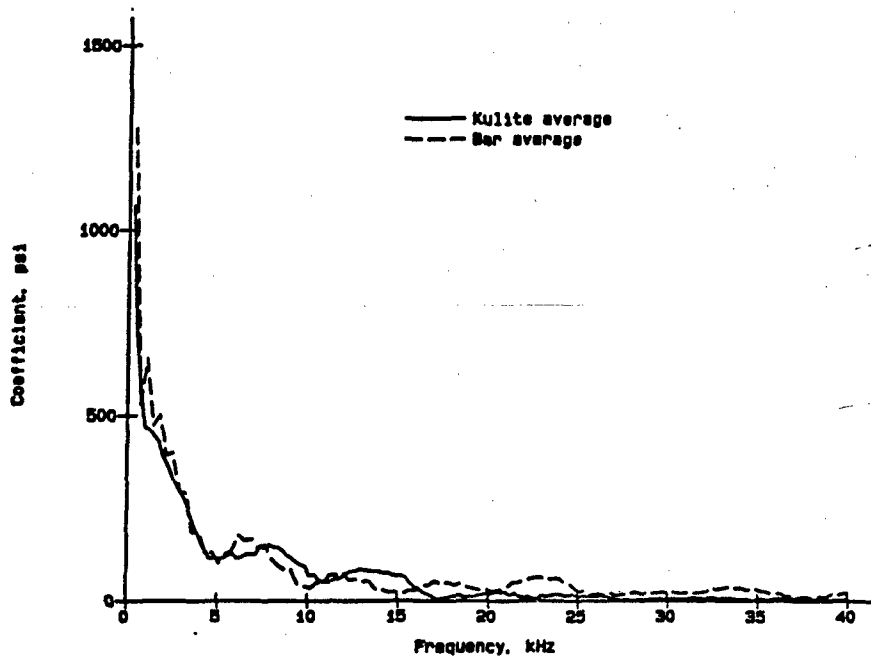


Figure 2.16. Frequency content of averaged Kulite and bar gage data.

## CHAPTER 3

### EFFECT OF WATER AND WATER SEAL

#### 3.1 BAR, WATER, AND WATER SEAL

All of the calculations performed (using only the bar) indicated that the late-time stresses measured by the bar gage should agree exactly with the PCB measurements. However, as indicated in Figures 1.2 and 1.3, late in time the two gage types disagree. Calculations including the water and water seal were performed to determine if they could be the reason for this late time difference.

The water was added to the grid as shown in Figure 3.1. The elements used to model the water were 1/10 in. thick in the vertical direction. The water began at the top of the grid and extended 48 in. down the bar. The outer boundary of the water was a roller boundary. On the inside, the water was allowed to slide without friction on the bar. The water seal was tied to the bottom of the water grid and the plastic seal was modeled as two 1/10-in.-thick elements.

In all of the calculations involving water, the water was modeled as an inviscid fluid using the following equation of state:

$$p = C (\rho/\rho_0 - 1)$$

Where:  $p$  is the pressure,

$C$  is a constant =  $3.973 \times 10^5$  psi

$\rho$  is the current density

$\rho_0$  is the initial density = 62.4 pcf

This is equivalent to a constant bulk modulus. In these calculations the plastic water seal was modeled as an elastic material with an elastic

modulus, Poisson's ratio, and density of 580,000 psi, 0.4, and  $1.120 \times 10^{-4}$  lb sec<sup>2</sup>/in.<sup>4</sup>, respectively.

Two calculations were performed using the PCB2 loading. In the first calculation, the water seal was free to slide on the bar. In the second calculation, the water seal was tied to the bar and fixed on the side of the PVC pipe. Figure 3.2 shows the early-time results of the calculation with the free water seal and the calculation using the bar only. The early-time stresses for the calculation using the tied water seal are identical to those using the free water seal, since the effects of the seal do not occur until later in time. This figure indicates that the presence of the water jacket does not cause a significant difference in the predicted peak stress.

Figure 3.3 shows a comparison of the calculations for the fixed and free water seals, and the calculation which does not include the water. The stresses at 6 ft down the bar are nearly identical until approximately 0.8 msec. At this time the stresses have propagated down the water to the water seal and those effects have propagated down the bar to the 6 ft level.

In the calculation where the water seal is free to move, the water seal suddenly moves and relieves the pressure in the water. This sudden release of water pressure causes a tensile strain to be propagated down the bar.

When the water seal is attached to the bar, the stresses propagate down the water to the water seal and the load is transferred to the bar. This results in the additional compressive stresses as shown in Figure 3.3. These stresses are similar in magnitude to the actual airblast stresses measured in the bar, and are much greater than those measured by the WES gage.

In the actual bar gage, the connection between the water seal and bar gage is somewhere between free and tied to the bar. Therefore it is expected

that the late-time stresses measured in the bar would be between those predicted based on the free and tied water seals. It is possible for the water seal to separate from the PVC and for the water to flow around the seal. Also the PVC pipe can expand which will decrease the water pressures, and will decrease the effects of the water seal on the bar gage measurement. These calculations demonstrate that after 0.8 msec, the higher stresses measured by the bar gages could be caused by stresses in the water transferred, through the water seal, to the bar.

### 3.2 EFFECT OF WATER VISCOSITY

During the test the water moves down the bar and it is possible that viscous forces caused by this motion could be important. Because a viscous slide surface was not available in DYNA3D, this effect could not be directly evaluated in the FE calculation. Therefore, simple calculations, using the results of the FE calculation with the free water seal, were performed to determine an upper bound on the effect of these viscous forces.

In these calculations, the flow distribution shown in Figure 3.4 was used. This assumes that the velocity profile is parabolic, with zero velocity at the bar and the PVC pipe, and the maximum velocity midway between the bar and PVC. The stress transferred to the bar is given by:

$$s = \text{visc} * dv/dx$$

Where:  $s$  is the shear stress transferred to bar

$dv/dx$  is the velocity gradient as shown in Figure 3.4

$\text{visc}$  is the viscosity of water =  $1.38 \times 10^{-7}$  lb sec/in<sup>2</sup>

This is the viscosity of water at 70 degrees Fahrenheit. For the assumed velocity distribution and the geometry of the bar gage, the value of  $dv/dx$  (per in.) at the surface of the bar is 8.0 times the peak velocity (ips).

The axial stress,  $a$ , in the bar caused by the viscous forces between the bar and water is given by:

$$a = s * p * L / A$$

where  $p$  is the perimeter of bar = 3.14 in.

$L$  is the length of contact between bar and water (48 or 72 in)

$A$  is the area of bar = 0.785 in<sup>2</sup>

Two calculations were performed to determine the effects of water viscosity on stresses in the bar. In either case, the velocity of the bar was conservatively neglected in computing the relative velocity between the bar and water. The velocity time-histories near the top and at the bottom of the column of water, based on the FE calculation, are shown in Figure 3.5.

In the first calculation, it was assumed that the entire 4 ft column of water was moving at the peak velocity, 8,000 ips, at the top of the water. This calculation should significantly overpredict the load transferred to the bar, since the duration of the peak velocity is extremely small and the peak velocity will only act over a very small portion of the length of the bar at any given time. For this case:

$$dv/dx = 8.0 \times 8,000 = 64,000 \text{ per sec}$$

$$s = 1.38 \times 10^{-7} \times 64,000 = 0.00883 \text{ psi}$$

$$a = 0.00887 \times 3.14 \times 48 / 0.785 = 1.70 \text{ psi}$$

In the second calculation, it was assumed that the water has spread out and now covers the top 6 ft of the bar and the water is moving at the spill velocity, 6,000 ips, of the bottom of the water. For this case:

$$dv/dx = 8.0 \times 6,000 = 48,000 \text{ per sec}$$

$$s = 1.38 \times 10^{-7} \times 48,000 = 0.00662 \text{ psi}$$

$$a = 0.00662 \times 3.14 \times 72 / 0.784 = 1.91 \text{ psi}$$

These calculations indicate that viscous forces transmitted to the bar from the water do not significantly affect the bar gage measurements.

Figure 3.6 shows the displacement of the top of the water minus the displacement of the top of the bar for the calculation in which the water seal is free to move. This figure indicates that only a very small portion of the top of the bar will be exposed to the airstream pressure. Since the area of bar exposed is so small, and since the air cannot be moving past the bar faster than the water, the effect of viscous flow of the air past the bar on the stresses measured by the bar is insignificant.

### 3.3 BAR, WATER, WATER SEAL, PVC PIPE, AND SOIL

Previous calculations including the bar, water, and water seal indicated that it is possible that late-time increases in the bar gage measurement could be due to loads transferred to the bar from the water seal. In these calculations, the water was not allowed to expand radially, and the seal was either free to slide on the bar, or was tied to the bar. To more accurately assess the effect of the water and water seal on the loads measured by the bar gage, the effects of the expanding water should be considered and a more accurate model of the connection between the water seal and bar should be used.

When the airstream pressure hits the top of the bar gage, it also hits the top of the water, PVC, and surrounding soil. The pressure transmitted down the water jacket to the water seal is affected by the expansion of the water jacket. The expansion of the water jacket is affected by the pressure in the water inside the water jacket, the material properties of the PVC, and the resistance to expansion provided by the surrounding soil. For this

reason, the bar, water, water seal, PVC pipe, and the surrounding soil should be included in the calculation.

The cross section of the grid used for these calculations is shown in Figure 3.7. The entire top surface was loaded uniformly with the PCB2 loading. The bar gage was modeled using the 1/10 in. grid, as was used previously. The only difference in the bar part of the grid for this run was that starting at 10 ft down the bar, the element thickness was gradually transitioned to 0.2 in. This was done to reduce the number of nodes and elements, since a large number of nodes and elements were needed to model the PVC and soil. The bottom of the bar was free to move in the vertical direction. The portions of the grid used to model the water and water seal were identical to those used in the previous calculations. In this calculation, the water and water seal can slide without friction on the bar.

Only the top 10 ft of the PVC pipe was modeled. Stresses travel much slower in the PVC, and only 10 ft of the PVC is needed for the time of interest of this calculation. The elements in the PVC pipe were 1/5 in. thick in the vertical direction, and two 0.1-in.-thick elements were used to model the 0.2-in. thickness of the PVC pipe. In the circumferential direction, the nodes in the grid for the PVC pipe matched up with those of the grid for the water. The PVC pipe and water seal were modeled as an elastic-perfectly-plastic material with a density, elastic modulus, Poisson's ratio, and yield strength of 87.3 pcf, 450,000 psi, 0.4, and 8,000 psi, respectively. The water and water seal were allowed to slide without friction on the inside of the PVC.

A 36-in.-thick ring of soil was placed around the PVC pipe. The soil extended to a depth of 6 ft below the top of the bar. The soil was free to

move in the vertical direction at the bottom of the soil grid. The outer boundary of the soil was a roller boundary. The soil elements were 1-in. thick in the radial and vertical directions. In the circumferential direction, the soil grid matched up with the grid used for the PVC pipe. The use of exact material properties for this study was not necessary. It was only necessary to select a material which would behave in a manner similar to the one used in the test. The material properties and a constitutive model fit [9] were available for a concrete sand tested in a previous test series. These properties were used.

The sand was modeled using a modified version of the cap model [10] developed by GA Technology, Inc., which was added to DYNA3D. In this model, plastic yielding occurs when the square root of the second invariant of the deviatoric stress tensor reaches the envelope defined by the tensile cutoff, the failure surface, and the elliptical cap. The model uses an associative flow rule. The tensile cutoff,  $T$ , and aspect ratio,  $R$ , of the cap are material properties which must be determined from laboratory test data. The failure surface is defined by:

$$Y = A - B \exp(-L * I_1) + H * I_1$$

Where:  $A$ ,  $B$ ,  $L$ , and  $H$  are material properties to be determined from laboratory test data

$I_1$  is the first invariant of the stress tensor

The elliptical cap is movable and its location is implicitly defined by the hardening function:

$$e_v^P = W [1 - \exp\{D_1 * (X - X_0) + D_2 * (X - X_0)^2\}]$$

Where  $e_v^P$  is the volumetric plastic strain

$W$  is the maximum volumetric plastic strain

D1, D2 are material constants

X, and X0 are the current and initial values of the intercept of the cap with the I1 axis

W, D1, D2, and X0 are all material constants which must be determined from laboratory tests. The elastic shear modulus, G, is a constant. The elastic bulk modulus varies with pressure, P, as follows:

$$K = K1 + K2 P^{K3}$$

Where K is the bulk modulus

K1, K2 and K3 are material constants.

The values used for each of these constants are listed in Table 3.1. For the soil material, twice the default values of the linear and quadratic artificial viscosity terms were used. Flanagan-Belytschko hourglass control (coefficient = 0.15) with exact volume integration was used for the soil. A maximum strain increment of 0.00001 was used for the soil. The soil was allowed to slide without friction on the PVC pipe.

In the DET Development test, the water seal was a 0.2-in.-thick plastic ring which fit around the bar and inside the PVC. The inner and outer edges of the ring were grooved to accept an o-ring. The o-ring on the outside of the water seal was installed during the test, but the fit of the water seal around the bar was so tight that the inner o-ring could not be installed. The o-ring groove on the inside of the water seal decreased the thickness of the water seal in contact with the bar to 0.1 in. Thus, the maximum load which could be transferred to the bar through the water seal was the shear strength of the water seal, times the perimeter of the bar, times 0.1. Therefore the maximum load which can be transferred is 0.314 times the shear strength of the water seal.

In these calculations a more realistic model of the connection of the water seal to the bar was needed. The water seal was installed by sliding it down the bar. A relatively small force was required to slide the seal down the bar, therefore, it was assumed that the frictional drag force of the seal on the bar was small. The only way which the ring could possibly load the bar significantly, was if the force required to slide the ring down the bar was related to the rate at which the seal was moved down the bar. Thus in the FE calculation, the water seal was connected to the bar using viscous springs. After the calculation, the maximum force transmitted to the bar was checked to assure that it did not exceed the shear capacity of the water seal.

Viscous springs are available in DYNA3D and these were used to connect the water seal to the bar and the PVC pipe. Five springs were used to connect the inside of the water seal to the outside of the bar. Their locations are marked S1 through S5 on Figure 3.1 Springs marked S6 through S10 connected the water seal to the PVC pipe. The nodes at the bottom of the water seal were connected to nodes on the bar and PVC pipe at the height of the top of the water seal. Because these springs represent a distributed shear force around the circumference of the bar and PVC pipe, and because the circumference of the PVC pipe is larger than that of the bar, the viscosity of the springs attaching the water seal to the PVC pipe must be higher than the viscosity of the springs attaching the seal to the bar. The viscosities of the springs connecting the seal to the PVC were 2.5 times the viscosities of the springs connecting the seal to the bar. Springs S1, S5, S6, and S10 are located on the symmetry planes of the grid, and thus, only represent half the area of the other springs, therefore the viscosity of these springs was

taken as half of the viscosity of the center springs. Since no information was available on the viscosity which should be used, an arbitrary value of 0.333 lbs/ips was selected. Based on this, and the above discussion the following values of viscosities were used:

| Springs    | Viscosity<br>lbs/ips |
|------------|----------------------|
| S1, S5     | 0.166                |
| S2, S3, S4 | 0.333                |
| S6, S10    | 0.416                |
| S7, S8, S9 | 0.832                |

This converts to a viscous force of 5.33 lbs per ips of relative velocity between the bar and the water seal.

Figure 3.8 shows a comparison of the results of this calculation with the bar gage data, and the results of the calculation using only the bar. The calculation became unstable at approximately 1.1 msec, therefore, the plot is terminated at that point. Until approximately 0.80 msec, the results of the calculation using the entire grid are nearly identical to those using only the bar. This time coincides with the travel time for a stress wave to propagate down through the water to the water seal, and from there down the bar to the strain gages.

The time of departure of the whole-grid calculation from the bar-only calculation agrees reasonably well with the results of the calculation using the bar, water, and water seal, with the water seal tied to the bar. In the calculation using the whole grid, however, the water seal can move significantly and relieve the pressure in the water. Thus the high pressure

spike which appeared in the predicted bar measurement in the bar-plus-water calculation does not occur in this calculation.

The stresses transmitted to the bar from the water seal were evaluated to insure that the shear capacity of the water seal was not exceeded. Figure 3.8 shows that the axial stress in the bar was increased by approximately 1,300 psi as compared to the bar only calculation. The added load contributed by the water seal is the area of the bar (0.785) times the stress in the bar. Thus the load added was 1,020 lbs. The shear stress is this load divided by the shear area (0.314) of the water seal. The shear area is the perimeter of the 1-in.-diameter bar times the 0.1 in. thickness of the water seal which is in contact with the bar. The shear stress applied to the water seal was 3,250 psi. The shear stress capacity is  $1/\sqrt{3}$  times the yield strength. Thus the shear strength of the PVC water seal is  $8,000/\sqrt{3} = 4,600$  psi. Therefore the shear strength of the water seal is not exceeded and the calculation is reasonable.

This calculation indicates that loads transmitted from the water through the water seal to the bar could be responsible for high stress readings in the bar at times after 0.8 msec after the top of the bar is loaded. Figure 3.8 shows that beginning at approximately 0.6 msec, the stresses recorded for the bar gage exceed those recorded for the PCB gage. The water alone cannot cause these differences.

A spacer block was placed inside of the water jacket at a distance of 2 ft down from the top of the bar. The effects of loading transferred from the water through this block to the bar could appear on the bar gage records at approximately 0.6 msec. This spacer block, shown in Figure 3.9, was designed to allow flow of the water past the spacer block and also to

minimize contact between the spacer block and the bar. The spacer block has a thickness of 0.25 in. and a contact area of approximately 0.125 in.<sup>2</sup> with the bar. Based on this contact area and the shear strength of the material, this spacer block could transfer a force of approximately 600 lbs. This would result in an increased axial stress measurement of 760 psi and could cause the difference (Figure 3.8) between the stresses measured in the bar gage and those predicted using the PCB gage loading. Further calculations are needed to study the flow through the block and loads transferred to the bar. This problem is primarily a fluid flow problem, and DYNA3D is not suitable for that calculation.

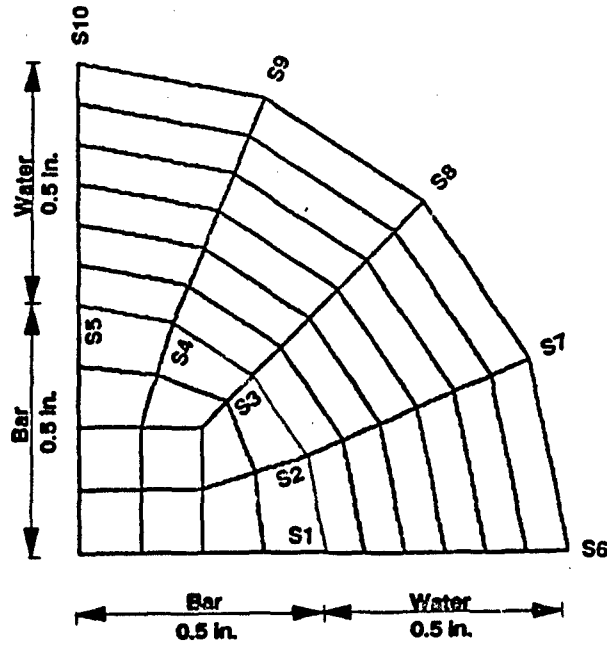


Figure 3.1. Water added to grid.

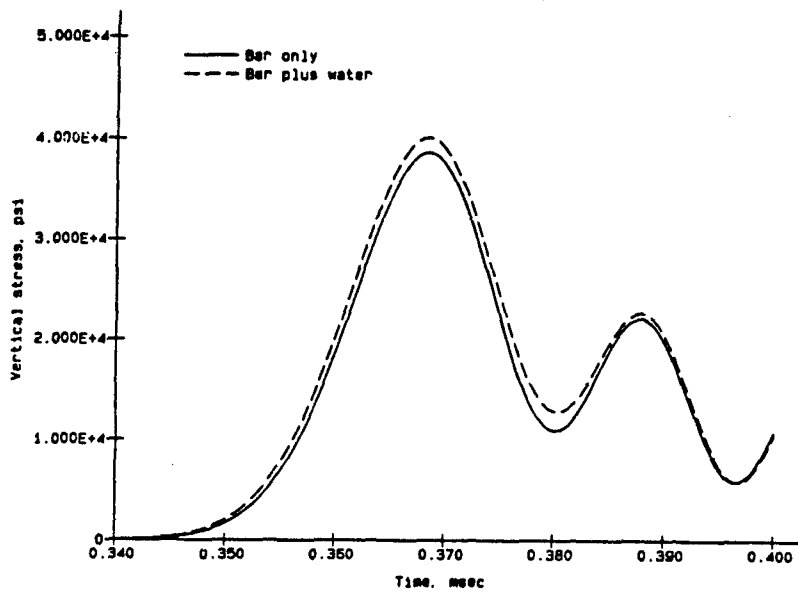


Figure 3.2. Early-time comparison of stresses with and without water.

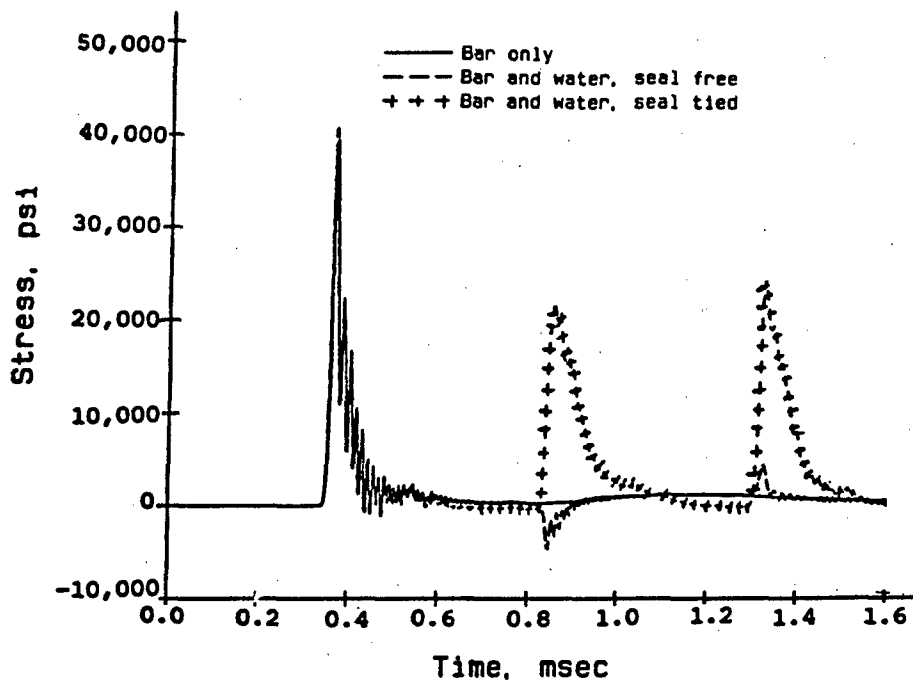


Figure 3.3. Comparison of bar stresses with and without water.

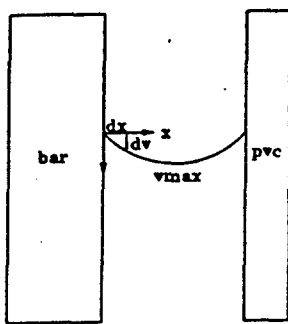


Figure 3.4. Velocity profile for viscosity calculations.

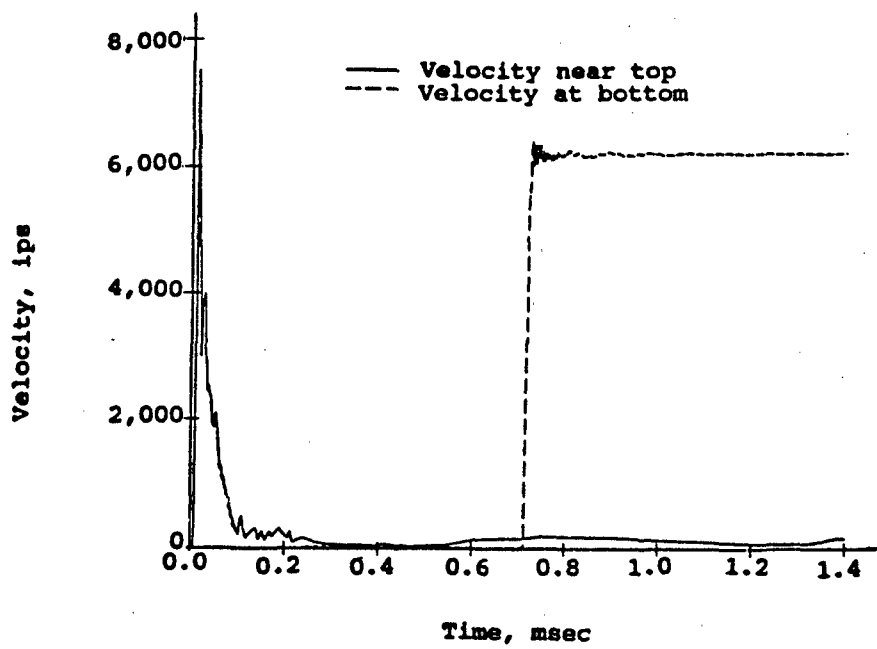


Figure 3.5. Velocities of top and bottom of water.

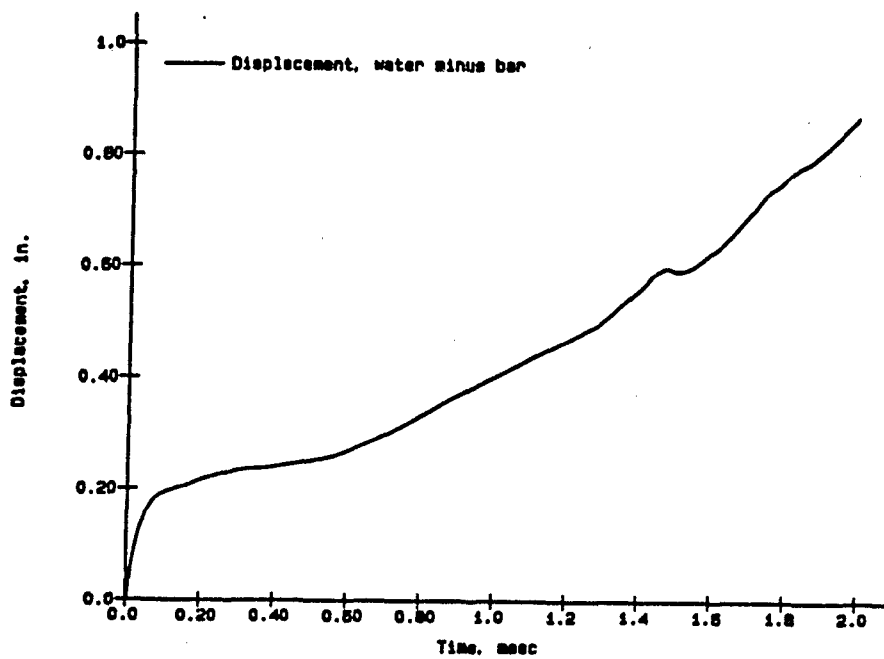


Figure 3.6. Relative displacement at top of bar.

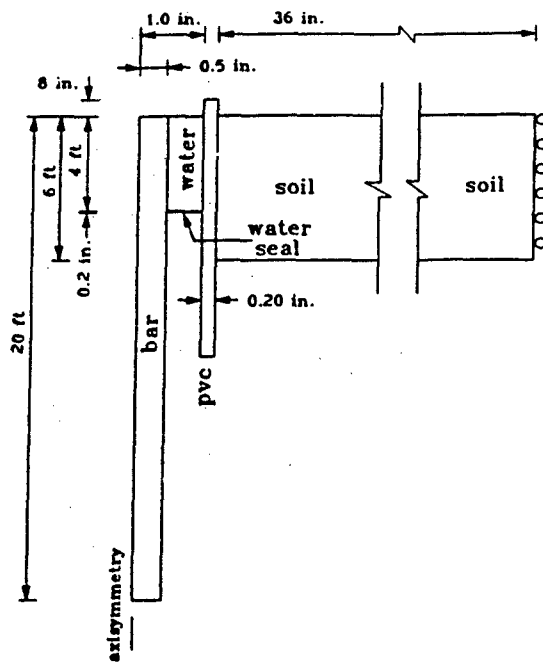


Figure 3.7. Section of grid including PVC pipe and soil.

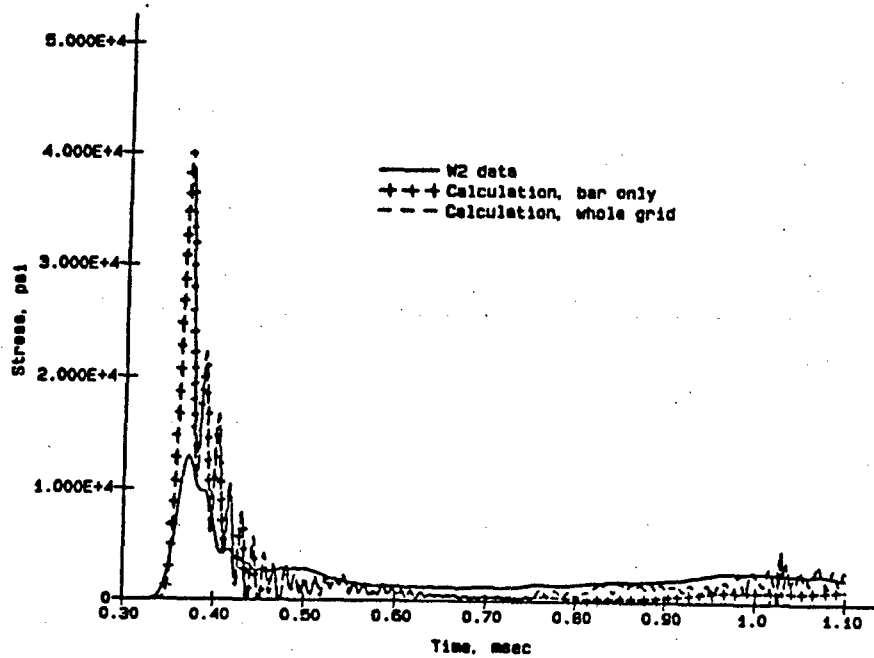


Figure 3.8. Bar stresses computed using entire grid.

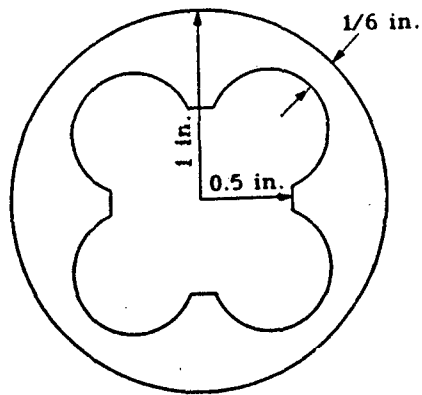


Figure 3.9. Spacer block.

## CHAPTER 4

### COMPARISON OF WES AND NMERI BARS IN DET DEVELOPMENT TEST

#### 4.1 REASON FOR ANALYSES

In the DET Development test, 5 WES and 5 NMERI bar gages were placed in the DET portion of the test bed. Five PCB gages were also placed in this portion of the test bed. The 5 WES gages showed that the pressure time-history had one dominant peak. The 5 NMERI gages showed that the pressure time-history had a dominant pair of peaks. Two of the PCB gages agreed with the single-peaked pressure time-history while two agreed with the double-peaked stress time-history. The fifth PCB gage failed very early in time. These gages were placed closely together and an attempt was made to eliminate systematic differences in the placement of different gage types.

The DET simulation was designed to produce an airblast which is spatially uniform. Although the PCB gages indicate that the character of the pressure time-history at one point in the bed is different than the character of the pressure time-history in another part of the bed, it seems highly unlikely that all of the WES bar gages were placed in areas where the airblast pressure time-history had a single peak and all of the NMERI bars were placed in areas where the time-history had a double peak. Therefore, it is reasonable to attempt to determine if differences between the two bar types could cause a systematic difference in the measured stress time-history.

The NMERI and WES bar gages fielded in the DET development test are summarized below:

| parameter        | WES                 | NMERI               |
|------------------|---------------------|---------------------|
| type             | high strength steel | high strength steel |
| diameter         | 1.0 in.             | 0.5 in.             |
| length           | 19 ft               | 20 ft               |
| strain gage type | semi-conductor      | foil                |
| distance to gage | 6 ft                | 5 ft                |

The WES bar gage data were recorded using cabling and electronic and recording equipment capable of a frequency response of approximately 20,000 Hz. The NMERI gages were recorded much closer to the test bed and the frequency response of these gages is somewhat better than that of the WES gages.

The "exact" theory of wave propagation in an elastic rod was used to compare the response of the WES and NMERI bar. The "exact" theory indicates that the NMERI bar should have a higher frequency response because of its smaller diameter. Less dispersion of the stress wave will occur in the NMERI bar because of the smaller bar and because the gage is placed closer to the top of the bar. The shorter travel distance will give the stress wave less time to disperse. The effects of these parameters were studied by calculating the response of the NMERI, as well as the WES bar, to the PCB2 and PCB3 loadings using the "exact" theory. PCB2 and PCB3 had single- and double-peaked records, respectively. The effect of the lower frequency response capability of the electronics used with the WES gage was also evaluated.

#### 4.2 RESPONSE TO PCB3 LOADING

The PCB3 pressure time-history was applied to the top of the WES and NMERI bars to predict the stresses that should have been measured by each of those gages. Figure 4.1 shows comparisons of the computed stresses for the NMERI bar to the PCB3 loading and the NMERI bar measurement, N4, from the test. These were time-shifted, and exact arrival times are meaningless. This plot shows that, based on "exact" theory, the stresses measured in the NMERI bar should have been nearly identical to the airblast measured by the PCB gage. The rise time to peak pressure should also be nearly the same. This figure shows that the peak measurement made by the NMERI bar gage, N4, is much less than the predicted peak and the rise time is much slower. It appears that the frequency response of the NMERI gage, and associated electronics, was somewhat less than that of the PCB gage.

Figure 4.2 shows the bar gage measurement, the "exact" solution and an filtered "exact" solution using only the Fourier series terms with a frequency of less than 20,000 HZ. This plot shows that the first peak is underpredicted if the calculated response is filtered to less than 20,000, and indicates that the frequency response of the NMERI bar gage system is probably greater than 20,000 Hz. Figure 4.3 shows the Fourier series coefficients for the PCB3 and N4 data records. Each of these was fit for a duration of 0.09 msec. This figure indicates that the history from PCB3 has significant energy at frequencies above 40,000 Hz, while the N4 record rolls off significantly at a frequency below 30,000 Hz.

Figure 4.4 shows comparisons of calculations for the NMERI bar and WES bar to the PCB3 loading. This figure indicates that the NMERI bar will have a shorter rise time and will record a higher peak than the WES bar gage.

The general characters of the pressure time-histories for the WES bar, the NMERI bar and the PCB gage are all the same. In each case a bar loaded with a double-peaked pressure pulse will indicate a double-peaked stress time-history in the bar.

Figure 4.5 shows a comparison of the PCB3 record and the "exact" solution for the WES bar filtered to 20,000 Hz. This figure shows that even with the lower frequency response, the WES bar will record a doubly-peaked stress time-history if it is loaded with the double-peaked pressure time-history of PCB3. The filtered prediction for the WES bar gage is not significantly different than the filtered prediction for the NMERI gage. This indicates that differences in the frequency response of the electronics used for each of the gages are more important than the physical differences in the two gage types.

#### 4.3 RESPONSE TO PCB2 LOADING

The response of the WES bar gage to the PCB2 loading has been thoroughly discussed in Chapters 2 and 3. Calculations were also performed to assess the response of the NMERI bar to the loading from PCB2. Figure 4.6 shows a comparison of the PCB2 data to the predicted responses for the WES bar and the NMERI bar. Again the NMERI bar has a faster calculated rise time and the peak stress in the NMERI bar is higher than that of the WES bar. This figure also shows that either bar could give a significant second peak, even when there is not one present in the airblast loading. This second peak is due to oscillations in the stress and which are a characteristic of the "exact" solution. These second and other peaks are not a problem since they could be eliminated by interpretation of the bar gage data using the "exact" solution. Figure 4.7 shows that when the two solutions are filtered to 20,000 Hz, there

is little difference between the predicted stresses. The significant second peak also disappears when the records are filtered. Thus, either gage type would record a single-peaked stress time-history if loaded with a single-peaked loading.

#### 4.4 OVERALL COMPARISON OF WES AND NMERI BAR GAGES

When the NMERI and WES bars are loaded with the same pressure time-history, the measured stress in the NMERI bar will be slightly higher than that measured by the WES bar. This is primarily due to the higher frequency response capability of the electronics, cabling and recording systems associated with the NMERI gages. There is also less dispersion in the NMERI bar.

The calculations indicated that when the WES and NMERI bar gages are loaded by the same pressure-time histories, the measured responses of each gage will be similar. This is supported by data from the WES and NMERI bars in the area not under the DET in the DET Development test. The measured pressure-time histories for those two gages were very close to each other. Thus it is concluded that the pressure-time histories loading the NMERI gages must be different in character than those loading the WES gages.

Since the 5 PCB gages were all essentially identical, it is reasonable to assume that if they were all subjected to the same environment they would all respond the same. In identical environments the flow conditions around identical gages and mounts should be identical; thus the gages should record the same pressures. Since half of the surviving PCB gages indicated a single-peaked pressure time-history, while the other half indicated a double-peaked history, there must have been some variation in the character of the pressure time-history within the test bed.

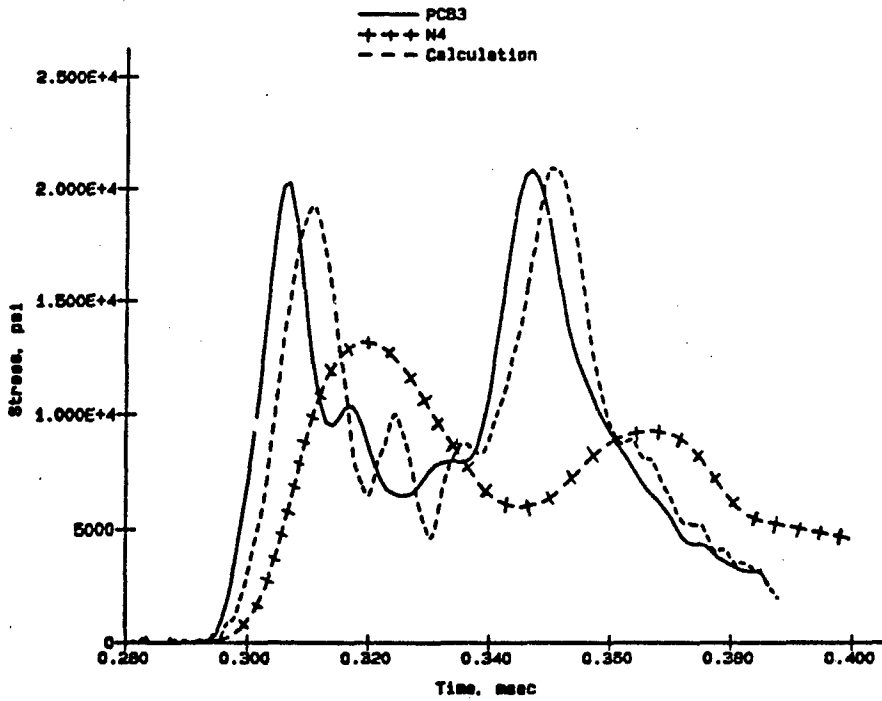


Figure 4.1. Comparison of PCB3 to N4 and "exact" solution for NMERI bar.

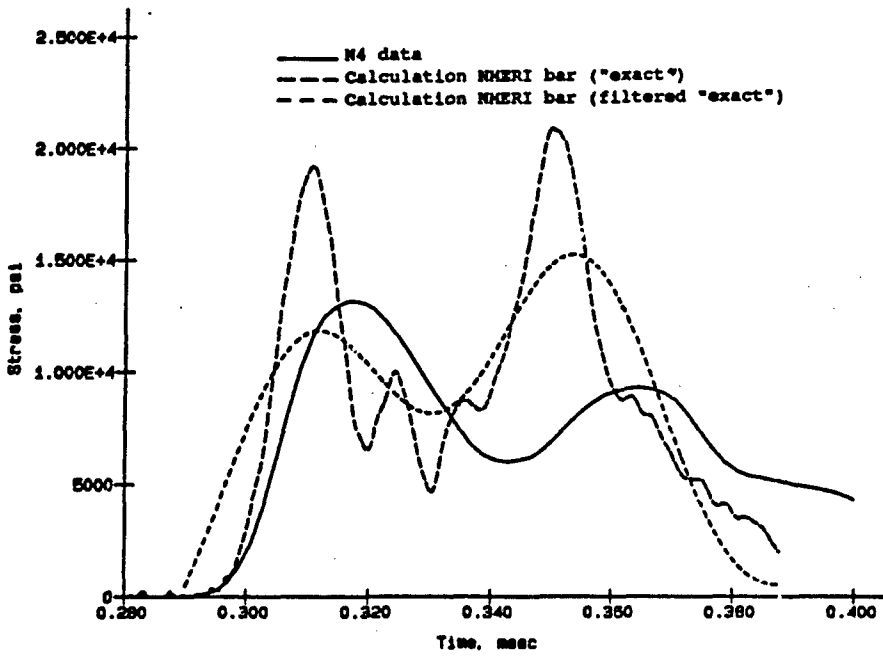


Figure 4.2. Comparison of N4 with "exact" and filtered "exact" solutions.

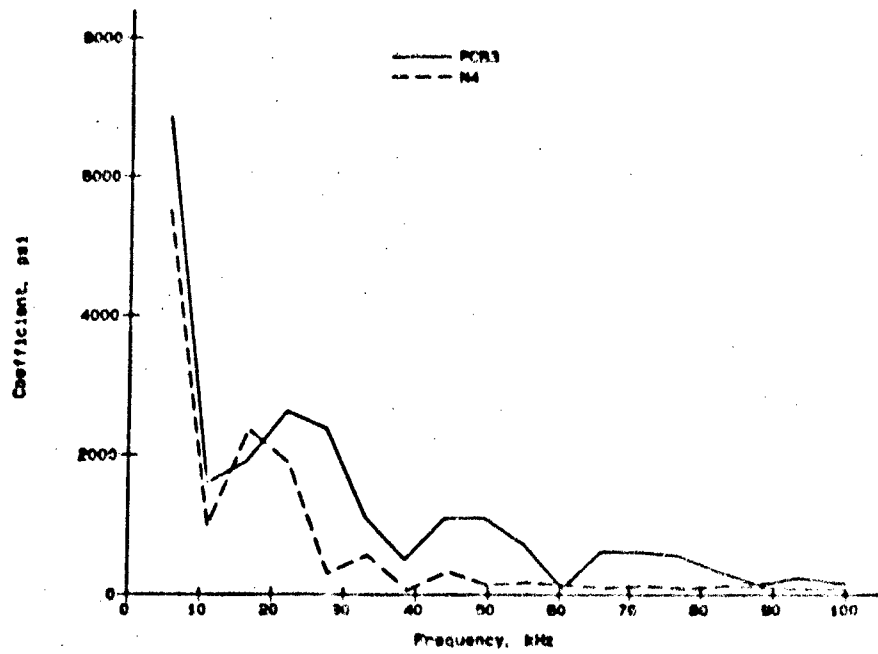


Figure 4.3. Fourier series coefficients for PCB3 and N4.

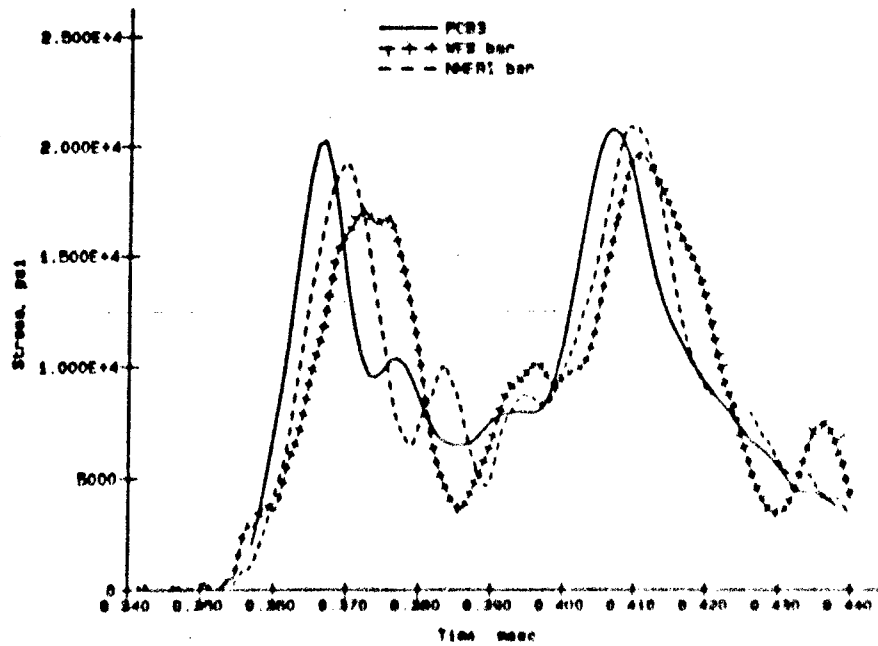


Figure 4.4. Comparison of PCB3 to "exact" solutions for WES and NMFRI bars.

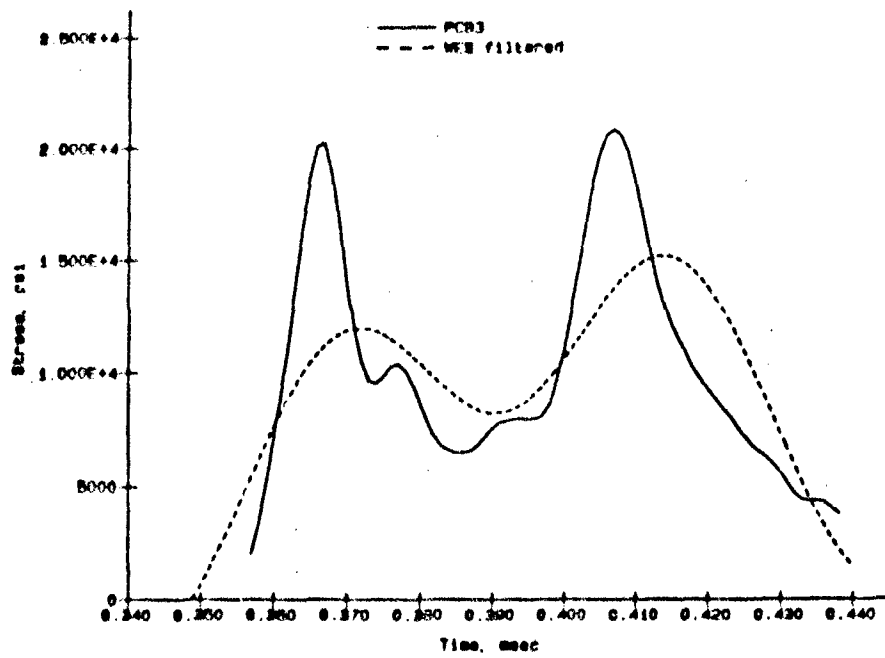


Figure 4.5. Filtered "exact" solution for WES bar, PCB3 loading.

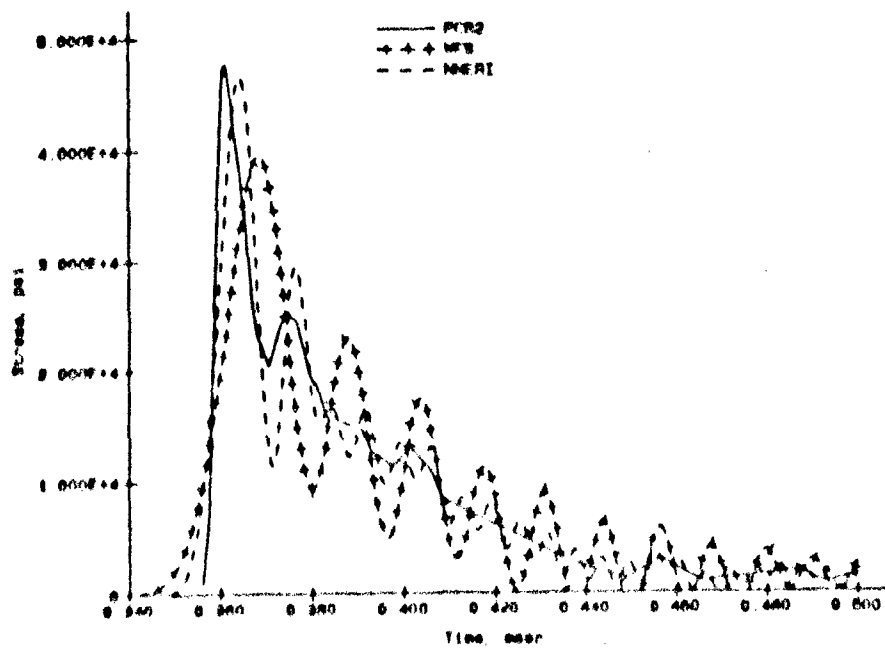


Figure 4.6. PCB2, "exact" solutions for WES and NMERI bars.

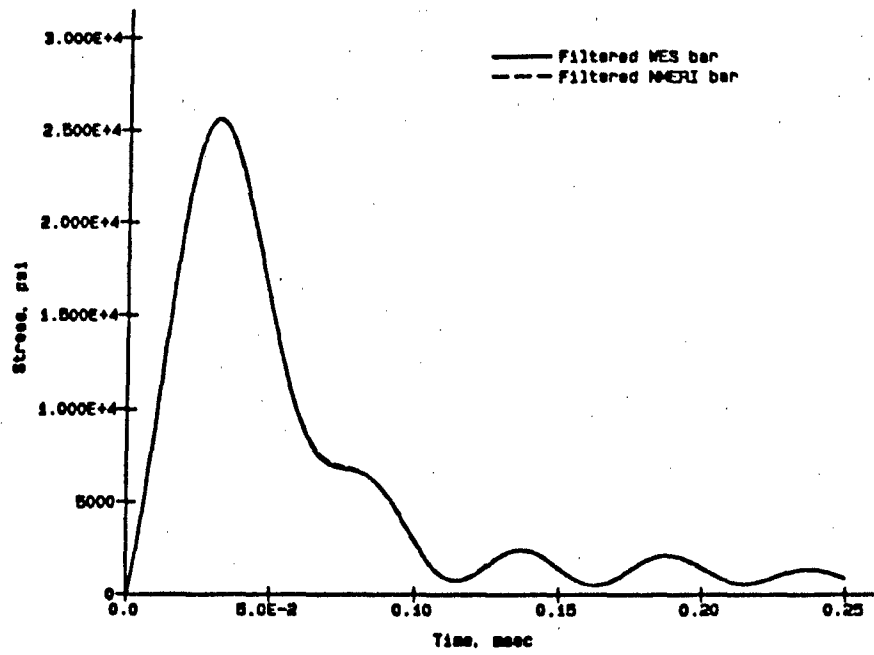


Figure 4.7. PCB2 filtered "exact" solutions for WES and NMERI bars.

## CHAPTER 5

### SUMMARY, CONCLUSIONS, AND RECOMMENDATIONS

#### 5.1 SUMMARY

Test data indicate that the peak stresses as measured by the WES bar gages were significantly lower than those measured by the PCB gages in the DET Development Test. The averaged peak stress for the WES bar gages in the Mineral Find III test was lower than the averaged peak stress for the Kulite pressure gages in that test. Later in time, the stresses measured by the WES bar gages were higher than those measured by the other gages in these two tests.

In the DET Development test, both WES and NMERI bar gages were used to measure airblast pressure. Five of each type of bar gage were used under the DET portion of the test bed. All 5 of the WES gages showed that the airblast pressure time-history had a single dominant peak, while all 5 of the NMERI gages indicated that there were two significant peaks. Two of the PCB gages agreed with the WES gages and two agreed with the NMERI gages. The fifth PCB gage failed.

When a high-frequency load is applied to the top of a bar, the stresses that propagate down the bar are affected by the radial motion caused by Poisson strains. The "exact" theory [4,5] accounts for this radial motion. Solutions for arbitrary loadings can be obtained using this theory and Fourier superposition. This method was used to analyze the response of the WES and NMERI bar gages and results compared extremely well with the results of FE calculations which included only the bar, thus validating the

FE procedures used. The theoretical solution was used to evaluate the response of the bar only.

The WES bar gage consists of the bar, a water jacket surrounding the top 4 ft of the bar, a PVC pipe which surrounds the water seal and bar, and a water seal which holds up the water jacket. The soil surrounding the PVC pipe could also affect the response of the bar. FE calculations were performed to assess the effects of the water, water seal, PVC pipe, and soil. Calculations were performed to assess the response of the WES bar gages in the DET Development test and the Mineral Find III test, and to assess the relative responses of the WES and NMERI gages in the DET Development test. In each calculation for the DET Development test, data from one of the PCB gages was used as the loading on top of the bar. In the Mineral Find III calculations, the averaged Kulite data were used as the loading. Although the accuracy of the loading on the top of the bar is limited by the accuracy of the PCB or Kulite gages, the results of these calculations do indicate the limitations of the bar gage.

## 5.2 CONCLUSIONS

The primary reason that peak stresses, as measured by the WES bar gages, are lower than those measured by the PCB gages in the DET development test is the lower frequency response capability of the cabling and recording equipment used with the bar gages. Dispersion in the bar and variability of the environment are responsible for part of this difference.

The bar gage should be just as accurate as the Kulite gages used in the Mineral Find III test since both gage types have approximately the same frequency response limits. Test data for this test showed that measured peak

stresses were higher for the Kulite gages than for the bar gages, but this trend did not hold true in previous tests in which both gage types were used. The presence of the water jacket does not significantly affect the peak stress measured in the bar.

Each of the gages used in these tests actually measures the airblast pressure above the gage itself, and not the actual pressure above the ground surface. Differences in the gages and their mounts, and the motion of the mount could be responsible for differences in the measured stresses. The movement of the water surrounding the bar and the flow of air into the void left by this moving water could affect the late-time airblast pressures applied to the top of the bar.

Viscous flow of the air past the end of the bar does not significantly affect the forces in the bar. Neither does drag of the water past the bar. However, significant stresses can be transmitted to the bar when the pressure propagates down the water and strikes the water seal at the bottom of the water jacket. This could be at least partially responsible for the late-time rise in stresses as seen in the bar gage data. These forces are of the correct magnitude but appear to arrive slightly later than the time at which the late-time increase in force occurs in the bar. However there is a spacer block located between the top of the bar and the water seal. Forces from this spacer block could arrive in time to cause the late-time increase in stress in the bar. The load caused by this spacer block is dominated by flow of the water through the block and DYNA3D is inappropriate for performing this calculation.

Because the cabling and electronics associated with the NMERI bars has a slightly higher frequency response limit than those associated with the WES

bar, the NMERI bars should record the pressure time history more accurately. The response of the NMERI bar itself is not significantly better than the response of the WES bar. The character of the measured pressure time-histories for the WES bar gages is different than that of the NMERI gages because the character of the airblast loading on the top of the WES bars is different than that of the NMERI bars.

### 5.3 RECOMMENDATIONS

Calculations are needed to assess the response of each of the gage types to the same environment. Each gage measurement is affected by the flow conditions around the gage and gage mount. These calculations are needed to determine if the different gage types should respond the same. Calculations should also be performed to determine the loads transferred to the bar that are caused by flow of water through the spacer block.

The loads on the bar gage are measured using strain gages that are places on flat spots on the bar. Calculations are needed to determine if these flat spots have a significant effect on the measured stress time-histories.

In future tests, efforts should be made to minimize the strength of the water seal. This will reduce the loads transferred to the bar. The tests should be recorded using cabling and recording equipment with a higher frequency response. If a system with a 50,000 Hz response was used the measured peak should be within 10 percent of the peak that actually occurs in the bar. A frequency response of 100,000 Hz should drop this error to approximately 2 percent.

Better methods [11] of interpreting bar gage measurements should be used. After the test, the gage should be turned back on, if possible, to determine if a shift in the zero-load output of the gage has changed. The bar should be inspected to determine if the spacer block and water seal have moved.

#### REFERENCES

1. C. M. Romander, and M. Sanai; "Development and Field Demonstration of Dilute Explosive Tiles (DET): Volume 1- DET Performance and Field Demonstration"; DNA-TR-91-84-V1, August, 1991; Defense Nuclear Agency, Alexandria, Virginia.
2. F. Roessler, "Mineral Find 1, 2, and 3, Volume II-Results," FCDNA Project Officer's POR 7356-2, October, 1991, Field Command, Defense Nuclear Agency, Kirtland Air Force Base, New Mexico.
3. J. O. Hallquist, and D. J. Benson; DYNA3D User's Manual (Nonlinear Dynamic Analysis of Structures in Three Dimensions); Report UCID-19592, July, 1987; Lawrence Livermore National Laboratory, University of California.
4. L. Pochhammer; "Uber die Fortpflanzungsgeschwindigkeiten kleiner Schwingungin in einem unbegrenzten istropen Kreiszyylinder"; Journal Reine Angew. Math, 81, 1876, pp 324-36.
5. Chree; "The Equations of an isotropic Elastic Solid in Polar and Cylindrical Coordinates, Their Solutions and Applications"; Trans. Camb. Phil. Soc. Math. Phys. Sci., Vol 14, 1889, p 250.
6. A. E. H. Love; Mathematical Theory of Elasticity; Cambridge Press, 1934.
7. D. Bancroft; "The Velocity of Longitudinal Waves in Cylindrical Bars"; Physical Review, Second series, Vol 59, 1941, p 588.
8. R. M. Davies; "A Critical Study of the Hopkinson Pressure Bar"; Phil. Trans. R. Soc., A240, 1948, pp 375-457.
9. J. T. Baylot; "Parameters Affecting Loads on Buried Structures Subjected to Localized Blast Effects"; Technical Report SL-92-9, April, 1992, U.S. Army Engineer Waterways Experiment Station, Vicksburg, Mississippi.
10. D. Pelessone; "A modified Formulation of the Cap Model"; Draft Report GA-C19579, January, 1989; General Atomics, San Diego, California; Prepared for the Defense Nuclear Agency, Alexandria Virginia.
11. D. A. Gorham; "A Numerical Method for the Correction of Dispersion in Pressure Bar Signals"; J. Phys. B: Sci. Instrum., Vol 16, 1983, pp 477-479.

DISTRIBUTION LIST FOR MINERAL FIND TESTS

DOD

Director, Defense Nuclear Agency, ATTN: ADDST(T), TDTR (Mr. Kennedy, MAJ Holm, Mr. Flohr), SPSS (CPT Abernathy), 6801 Telegraph Road, Alexandria, VA 22310-3398

Commander, Defense Nuclear Agency, ATTN: FCX (Dr. Leech), FCTT (LTC Leners, Mr. Martinez, CPT Smith, CPT Scott (4 cys), Dr. Rinehart, CPT Roessler; NMHE (LCDR Taylor, LCDR Myers, CPT Dunn), Kirtland AFB, NM 87115-5000

AIR FORCE

Commander, Ballistic Missile Office, ATTN: MGEM (LT Cooper), Norton AFB, CA 92409-6458

ARMY

Director, U.S. Army Engineer Waterways Experiment Station, ATTN: CEWES-SE (Mr. L. K. Davis, Mr. J. Ingram, Mr. D. Rickman, Mr. J. Stout, Mr. C. Welch), CEWES-SS (Mr. F. Dallriva, Mr. J. Davis, Mr. P. Graham), CEWES-SD (Dr. J. Zelasko, Mr. B. Phillips), P.O. Box 631, Vicksburg, MS 39180-0631

Director, U.S. Army Ballistic Research Lab, ATTN: SLCBR-TB-B (Dr. Mark, Dr. Polk, Mr. Sullivan), Aberdeen Proving Ground, MD 21005-5066

Director, U.S. Army Missile and Space Intelligence Center, ATTN: AIAMS-YTT (Mr. Blanchard), Redstone Arsenal, AL 35898-5500

NAVY

Commander, Naval Research Laboratory, ATTN: Code 4040 (Dr. Book), Washington, DC 20375-5000

Commander, Naval Research Laboratory, ATTN: Code 6303 (Mr. Simpson), Washington DC 20375-5000

Commander, Naval Weapons Center, ATTN: Code 326 B, China Lake, CA 93555

Commander, Naval Weapons Evaluation Facility, ATTN: Mr. Alderete, Kirtland AFB, NM 87117

OTHER GOVERNMENT AGENCIES

Sandia National Laboratories, Albuquerque, ATTN: Mr. T. Herther (315), Mr. H. Church (6321), Mr. J. Reed (7111), Mr. Jinzo, Albuquerque, NM 87185

OTHER AGENCIES

Aberdeen Research Center, ATTN: Mr. Keefer, Mr. Ethridge, P.O. Box 548,  
Aberdeen, MD 21001

Carpenter Research Corporation, ATTN: Mr. Carpenter, P.O. Box 2490,  
Rolling Hills Estate, CA 90274

California Research and Technology, Inc., ATTN: Dr. Stockham,  
1900 Randolph Road, SE, Suite B, Albuquerque, NM 87106

California Research and Technology, Inc., ATTN: Mr. J. Thomsen,  
5117 Johnson Drive, Pleasanton, CA 94566

California Research and Technology, Inc., ATTN: Mr. Martin Rosenblatt,  
Dr. R. England, 20943 Devonshire Street, Chatsworth, CA 91311-2376

California Research and Technology, Inc., ATTN: Mr. Rocco, 520 B  
Wheeler SE, Albuquerque, NM 87102

Director, New Mexico Engineering Research Institute/CERF,  
ATTN: Dr. Baum, Mr. Schneider, Kirtland AFB, NM 87115

H-TECH Laboratories, Inc., ATTN: Mr. Hartenbaum, P.O. Box 1686,  
Santa Monica, CA 90406

Information Science, Inc., ATTN: Dr. Dudziak, 123 West Padre Street,  
Santa Barbara, CA 93105

Karagozian and Case, ATTN: Mr. Wesevich, Mr. Valoncins, 620 N Brand  
Blvd, Glendale, CA 91203.

Los Alamos Technical Associates, ATTN: Mr. McKee, 5301 Central, NE,  
Suite 751, Albuquerque, NM 87108

Particle Measurement Systems, ATTN: Mr. Robert Knollenberg, 1855 South  
57th Court, Boulder, CO 80301

Research & Development Associates, ATTN: Dr. Kuhl, Mr. Mazzola,  
P.O. Box 9695, Marina del Rey, CA 90291

Research & Development Associates, ATTN: Dr. Ganong, P.O. Box 9335,  
Albuquerque, NM 87119

Science Applications International, Corporation, ATTN: Dr. Cockayne,  
1710 Goodrich Drive, P.O. Box 1303, McLean, VA 22101-1303

S-Cubed, ATTN: Mr. Needham, P.O. Box 8243, Albuquerque, NM 87198

Tech Reps Inc., ATTN: Mr. F. McMullan, 5000 Marble Avenue, NM, Suite  
222, Albuquerque, NM 87110

Washington Research Center, ATTN: Mr. Flory, P.O. Box 2232,  
Springfield, VA 22152

Weidlinger Associates, ATTN: Dr. Levine, 4410 Camino Real, Suite 110,  
Los Altos, CA 94022

**REPORT DOCUMENTATION PAGE**

Form Approved  
OMB No. 0704-0188

Public reporting burden for this collection of information is estimated to average 1 hour per response, including the time for reviewing instructions, searching existing data sources, gathering and maintaining the data needed, and completing and reviewing the collection of information. Send comments regarding this burden estimate or any other aspect of this collection of information, including suggestions for reducing this burden, to Washington Headquarters Services, Directorate for Information Operations and Reports, 1215 Jefferson Davis Highway, Suite 1204, Arlington, VA 22202-4302, and to the Office of Management and Budget, Paperwork Reduction Project (0704-0188), Washington, DC 20503.

|                                  |                                |  |
|----------------------------------|--------------------------------|--|
| 1. AGENCY USE ONLY (Leave blank) | 2. REPORT DATE<br>January 1993 | 3. REPORT TYPE AND DATES COVERED<br>Final report |
|----------------------------------|--------------------------------|--|

|  |  |
|--|--|
| 4. TITLE AND SUBTITLE<br><br>Analysis of Hopkinson Bar Pressure Gage | 5. FUNDING NUMBERS<br><br>DNA Subtask RS RC/Missile System Vulnerability Work Unit 10186<br>FCDNA Project H42KRHRD Work Unit 80850 |
|--|--|

|                                     |  |
|-------------------------------------|--|
| 6. AUTHOR(S)<br><br>James T. Baylot | 8. PERFORMING ORGANIZATION REPORT NUMBER<br><br>Technical Report SL-93-1 |
|-------------------------------------|--|

|   |  |
|---|--|
| 7. PERFORMING ORGANIZATION NAME(S) AND ADDRESS(ES)<br><br>US Army Engineer Waterways Experiment Station, Structures Laboratory, 3909 Halls Ferry Road, Vicksburg, MS 39180-6199 | 10. SPONSORING/MONITORING AGENCY REPORT NUMBER |
|---|--|

|  |  |
|--|--|
| 9. SPONSORING/MONITORING AGENCY NAME(S) AND ADDRESS(ES)<br><br>Defense Nuclear Agency<br>Washington, DC 20305-1000 | 10. SPONSORING/MONITORING AGENCY REPORT NUMBER |
|--|--|

11. SUPPLEMENTARY NOTES  
  
Available from National Technical Information Service, 5285 Port Royal Road, Springfield, VA 22161.

|   |                        |
|---|------------------------|
| 12a. DISTRIBUTION / AVAILABILITY STATEMENT<br><br>Approved for public release; distribution is unlimited. | 12b. DISTRIBUTION CODE |
|---|------------------------|

13. ABSTRACT (Maximum 200 words)

U.S. Army Engineer Waterways Experiment Station (WES) designed Hopkinson pressure bar gages were fielded on the Dilute Explosive Tile (DET) test along with New Mexico Engineering Research Institute (NMERI) designed bar gages and pressure gages manufactured by PCB Piezotronics, Inc. On the Mineral Find 3 (MF3) explosive test, WES bar gages were fielded along with pressure transducers manufactured by Kulite. The peak pressures recorded by the PCB gages were much higher than those recorded by the WES bar gages on the DET test. The peak stresses were higher for the Kulite gages than for the WES bar gages in the MF3 test. In each of these tests, the stresses recorded later in time for the bar gage were higher than those recorded for the other types of gages.

The NMERI gages indicated that the pressure time-history had two significant peaks while the WES gages indicated only one significant peak. One-half of the surviving PCB gages agreed with the WES gages, while one-half agreed with the NMERI gages.

(Continued)

|   |                                  |                           |
|---|----------------------------------|---------------------------|
| 14. SUBJECT TERMS<br>Airblast pressure<br>Elastic wave propagation<br>Finite element analysis | Hopkinson bar<br>Instrumentation | 15. NUMBER OF PAGES<br>66 |
|   |                                  | 16. PRICE CODE            |

|   |  |   |                            |
|---|--|---|----------------------------|
| 17. SECURITY CLASSIFICATION OF REPORT<br>UNCLASSIFIED | 18. SECURITY CLASSIFICATION OF THIS PAGE<br>UNCLASSIFIED | 19. SECURITY CLASSIFICATION OF ABSTRACT | 20. LIMITATION OF ABSTRACT |
|---|--|---|----------------------------|

3. (Concluded).

Analytical and finite element (FE) calculations were performed to assess the response of the bar gages in these tests. The analytical solutions included only the bar and agreed extremely well with comparable FE calculations. These calculations indicated that the primary reason for the low peak stress readings in the bar gages was the lower frequency response capability of the recording system used to record the bar gage data.

The calculations also indicated that the presence of water around the bar did not significantly affect the measured peak stress in the bar, and that the drag of the water past the bar did not cause significant forces to be developed in the bar. It appears that the late time rise in the stresses measured by the bar gages was due to the spacer block and water seal sliding down the bar.

The calculations also indicated that the response of the NMERI bar gage should not be significantly different than the response of the WES bar gage. Therefore, it is concluded that the difference in character of the pressure time-histories between the two gage types is due to differences in character of the loading applied to the different gage types.

END

FILMED

DATE:

4-93

DTIC